PERGAMON

Applied Radiation and Isotopes 50 (1999) 39–62

Applied Radiation and Isotopes

Use of the concept of energy imparted in diagnostic radiology

Gudrun Alm Carlsson [a,*], David R. Dance [b], Jan Persliden [a], Michael Sandborg [a]

[a] *Department of Radiation Physics, IMV, Faculty of Health Sciences, SE-581 85 Linkoping, Sweden*
[b] *Department of Physics, The Royal Marsden NHS Trust, Fulham Road, London SW3 6JJ, U.K.*

Abstract

The concept of energy imparted by ionizing radiation to the matter in a volume is analyzed and methods to determine the energy imparted ε to the patient are reviewed, in particular, determinations based on measurements of the air kerma integrated over beam area [the kerma-area-product (KAP)] and calculations needed to derive conversion factors ε/KAP. The energy imparted to the image receptor, ε_{rec}, including the statistical aspects of the concept, and the effect of ε_{rec} on image quality and patient dose are also analysed. Finally, use of the energy imparted to the patient as a risk indicator is discussed.

1. Introduction

The energy imparted, ε, by ionizing radiations to the matter in a volume is the fundamental quantity of radiation dosimetry (ICRU, 1980). From this quantity, absorbed dose is derived as the expectation value, $\bar{\varepsilon}$, of the energy imparted per unit mass to a vanishingly small volume. While absorbed dose is a point quantity, taking a value at each point of an irradiated medium, the energy imparted requires specification of a volume. All radiation sensitive detectors (including the human body) are finite in size and their signals are related to the energy imparted or the spatial mean of the absorbed dose ($\bar{D} = \bar{\varepsilon}/M$, where M is the mass of the detector) rather than to absorbed dose.

The energy imparted to a volume is a stochastic quantity due to the stochastic nature of the emission of ionizing particles from their sources and the interactions of ionizing particles with matter and can be expressed in terms of the number of energy impartation events (ICRU, 1980; Alm Carlsson, 1985) and the energy imparted in each event. The latter concepts are used in a physical description [complementary to the linear energy transfer (ICRU, 1970)] of radiation quality (ICRU, 1983; Kellerer, 1985) with respect to the efficiency with which imparted energies are converted to measureable signals: heat (temperature rise), ion pairs in a gas, electron–hole pairs in a solid, emission of light (fluorescence, thermoluminescence), number of chemical changes of a given chemical specimen, biological response (DNA single and double strand breaks, risk of cancer induction etc.). Brenner (1989) discussed, within this framework of (microdosimetric) concepts, the radiobiological effectiveness of diagnostic X-rays and implications to risk estimates for breast cancer induction in mammography. The same concepts have been used in studies of the stochastic nature (quantum noise) of the energy imparted to image receptors (Swank, 1973; Dick and Motz, 1981; Chan and Doi, 1984; Sandborg, 1993a).

In the early days of diagnostic radiology, skin burns from Roentgen diagnostic examinations were not

* To whom all correspondence should be addressed.

0969-8043/98/$19.00
PII: S0969-8043(98)00087-6

uncommon. Absorbed doses to the skin were soon successfully reduced far below threshold values by introducing appropriate filtration of the primary X-ray beam. Even so, the entrance skin absorbed dose, the highest local absorbed dose in an X-ray beam, remained the quantity of choice for assessing the radiation burden to the patient in diagnostic examinations. It was thus used in the search for methods to achieve dose reduction and to optimise radiographic techniques (Henriksson, 1967). This practice favoured use of high kV techniques at the cost of image contrast, an important image quality parameter.

In the early fifties, it was realised that the increased risk of cancer induction and genetic injury after irradiation was a matter of prime concern to society. In a first attempt to estimate the stochastic risk from X-ray examinations, Feddema and Oosterkamp (1953) introduced the concept of energy imparted and presented a method to measure the energy imparted by registering the field size. In the sixties, experimental equipment in the form of plane parallel ionisation chambers was developed (Reinsma, 1962; Pychlau and Pychlau, 1964; Carlsson, 1965) for real time monitoring of the energy imparted to the patient. Such equipment is now commercially available and increasingly used for patient dosimetry. A protocol for calibration of the equipment, including requirements on maximum uncertainties, has been published by NRPB (1992). This reflects a general trend towards requirements on increased accuracy in patient dosimetry in diagnostic radiology (IAEA, 1994).

Initially the chambers were used to determine the energy imparted to the patient. Suitable conversion factors were derived using experimental methods and later Monte Carlo techniques. Today conversion factors are increasingly being expressed in terms of effective dose E (ICRP, 1991). Tabulations have been published which give conversion factors for both effective dose and energy imparted to the patient using anthropomorphic phantoms (Hart et al., 1994, 1996). The energy imparted has the attractive feature of being a physical quantity and not subject to uncertain estimates of biological effects. Also, conversion factors for energy imparted to the patient as derived for simple (homogeneous) phantoms have been shown to give results in good agreement with those derived using more sophisticated, anthropomorphic phantoms (Alm Carlsson et al., 1984; Carlsson and Alm Carlsson, 1990; Gkanatsios and Huda, 1997). In complicated procedures involving fluoroscopy, in CT examinations and in dental radiography involving small irradiated volumes, the energy imparted to the patient is likely to remain the quantity of choice (Stenström et al., 1987; Huda and Atherton, 1995; Huda et al., 1997; Helmrot, 1996) for practical optimizations of image quality and patient dose. For instance, Sandborg et al. (1993b) showed that in the optimization of an adult lumbar spine examination with respect to various physical parameters, the results were little influenced by using the energy imparted to the patient/phantom instead of effective dose as risk descriptor.

The concept of energy imparted is useful not only in estimating the stochastic risks of cancer induction and hereditary effects but also in predicting the response of image receptors in different conditions of irradiation. This review on the use of the concept of energy imparted in diagnostic radiology therefore focuses on two issues: determination of the energy imparted to the patient for risk estimates and the energy imparted to image receptors for predicting image quality. Patient dose and image quality are the main components to be considered in the optimisation of diagnostic radiology, which is a most important task for the radiation protection of the patient. In an optimised imaging system, quantum noise should be the factor limiting image quality (Motz and Danos, 1978). With the event of digital radiography, it has become possible to explore this limit in practice. The fundamental role of quantum noise in image formation points to the importance of understanding the stochastics of the basic processes of energy impartation events in the image receptor. In conventional radiography, the energy absorption properties of the receptor also have a major influence on the resulting image contrast (Wagner, 1977; Kalender, 1981; Nielsen and Carlsson, 1984; Tapiovaara and Wagner, 1985; Sandborg and Alm Carlsson, 1992; Sandborg et al., 1995). The energy absorption properties of the image receptor thus influence image quality in both digital and conventional screen-film imaging.

2. The energy imparted to the matter in a volume

2.1. Definition

The energy imparted, ε, to the matter in a volume is defined by the ICRU (ICRU, 1980):

$$\varepsilon = R_{in} - R_{out} + \sum Q \quad (1)$$

where R_{in} = the radiant energy incident on the volume, i.e. the sum of the energies (excluding rest energies) of all those charged and uncharged ionizing particles which enter the volume, R_{out} = the radiant energy emerging from the volume, i.e. the sum of the energies (excluding rest energies) of all those charged and uncharged ionizing particles which leave the volume, ΣQ = the sum of all changes (decreases:positive sign, increases:negative sign) of the rest mass energy of

nuclei and elementary particles in any nuclear transformations which occur in the volume.

The energy imparted ε is a stochastic quantity due to the statistical fluctuations in the number and type of interaction processes occurring in the volume.

2.2. Physical interpretation

From the definition it follows that energy imparted excludes the radiant energy which through interactions in the volume is converted into rest mass energy of nuclei and elementary particles, being subtracted through the term ΣQ. This type of energy conversion is not considered to contribute to the physical, chemical or biological effects of ionizing radiation which are instead considered to be wholly related to the energy transferred to the electronic structure of the medium, starting with ionizations and excitations of atoms and molecules. Through secondary processes, the ionizations and excitations may be further converted into energy forms suitable for detection (heat, light, changes of chemical bonds and damage to biological molecules). However, for the energies (<200 keV) and particle types (photons and electrons) relevant to diagnostic radiology, nuclei reactions or elementary particle transformations do not occur and, in this case, $\Sigma Q = 0$.

2.3. Absorbed dose

The absorbed dose, D, is the mean energy imparted (=expectation value of the energy imparted), $\bar{\varepsilon}$, per unit mass to an infinitesimal volume (ICRU, 1980)

$$D = \frac{1}{\rho} \lim_{V \to 0} \frac{\bar{\varepsilon}}{V} \tag{2}$$

where ρ is the density of the medium in volume V. Conversely, when the absorbed dose distribution in a volume is known, the mean energy imparted (expectation value of energy imparted) to that volume may be obtained from

$$\bar{\varepsilon} = \int_V \rho \cdot D \, \mathrm{d}V = \int_M D \, \mathrm{d}m \tag{3}$$

where M is the mass of volume V.

In the past, the mean energy imparted to a volume has also been called volume dose, integral dose, integral absorbed dose or total energy absorbed in the body.

3. Application to patient dosimetry

3.1. Brief historical review

The concept of energy imparted for patient dosimetry was first introduced by Mayneord (1940) in reaction to the radiation protection regulations then in force. These were based on the concept of dose at a point and Mayneord argued that the energy imparted to the body or to an organ, $\int_M D \, \mathrm{d}m$ (cf. Eq. (3)) should be a better estimator of general radiation effects than the dose in a single point, the latter taking no account of the size of the volume irradiated. He also suggested the use of average dose, i.e. the mean energy imparted divided by mass ($\bar{D} = \bar{\varepsilon}/M$).

Since then, energy imparted has been widely used in radiation therapy for determination of the efficiency (defined as the ratio of tumour dose to energy imparted) of different radiation qualities (conventional X-rays, ^{60}Co-gamma rays and X-rays from linear accelerators) (Mayneord and Clarke, 1975).

The concept of energy imparted was introduced into diagnostic radiology by Feddema and Oosterkamp (1953). They developed a method to measure the energy imparted to patients undergoing X-ray examinations and used it to make measurements in the clinic. The energy imparted was recorded by noting the field size, which was determined using potentiometers on the beam-defining collimators. This work attracted little attention. At that time, measurements of gonad absorbed doses for estimating the genetic effects of X-ray examinations on the population dominated the interest. The induction of cancer among the atomic bomb survivors increased the interest in somatic doses in X-ray diagnostics. In the early sixties, flat ionization chambers with an area larger than that of the maximum field were constructed (Reinsma, 1962; Pychlau and Pychlau, 1964; Carlsson, 1965) and calibrated to measure air collision kerma integrated over beam area $\int_A K_{\mathrm{c,air}} \, \mathrm{d}A$ (Pychlau and Pychlau, 1964; Carlsson, 1965). The chamber reading was converted to energy imparted to the patient using methods reviewed in Section 3.2. Today, the conversion factors are mainly calculated using Monte Carlo methods which are described and reviewed in Section 3.3.

3.2. Derivation of the energy imparted to the patient from physical measurements

The energy imparted to the patient can be derived by measuring the distribution of absorbed dose in the patient and integrating as in Eq. (3) or by using the definition in Eq. (1), i.e. measuring the radiant energies incident on and escaping from the patient.

In applying the second method, the incident radiant energy, R_{in} (Eq. (1)), can be derived using the above

cited measurements of air collision kerma integrated over beam area[1]. The measurements are consequently often named KAP (kerma area product) or DAP (dose area product) meters. A comprehensive review of the use and problems in KAP meter measurements has been given by Carlsson and Alm Carlsson (1990). In Section 3.2.1, methods to derive the energy imparted from absorbed dose distributions are reviewed. In Section 3.2.2, important aspects of KAP meter calibrations and the derivation of conversion factors, ε/KAP, are discussed.

3.2.1. Use of measured absorbed dose distributions

3.2.1.1. Measurements of absorbed dose distributions in a phantom. Mayneord and Clarkson (1944a,b) reported on measurements of energy imparted to the patient using a large number of small ionisation chambers distributed in a phantom. Boag (1945) used a body shaped detector that also served as a phantom.

More recently, Huda (1984) and Stenström et al. (1986) used large numbers (500 and 155, respectively) of thermoluminescent LiF dosimeters to measure the absorbed dose distributions in an Alderson phantom. These were integrated to derive the energy imparted to the patient from CT-examinations and intra-oral radiography. Almén and Nilsson (1996) used elliptically shaped water phantoms to simulate children of various ages and measured the dose distribution within the phantoms using LiF dosemeters. Mean absorbed doses in the organs were determined by averaging the measured absorbed doses obtained in the organ volumes, the size and position of which were identified using data from Cristy and Eckerman (1987).

3.2.1.2. Use of central axis depth–dose distributions: the saturated-scatter method. The saturated-scatter method (Happey, 1940, 1941) simplifies the determination of energy imparted to the patient as simulated by water phantoms. The energy imparted is approximated by (cf. Eq. (3))

$$\bar{\varepsilon} = \int_M D\,\mathrm{d}m \approx \rho \cdot A_0 \int_0^L D(x)\left(\frac{F+x}{F}\right)^2 \mathrm{d}x \qquad (4)$$

Here, ρ is the density, A_0 the field area at the surface, F the focus-to-surface distance, L the thickness of the phantom and $D(x)$ the absorbed dose on the central axis at depth x. Integration is performed over the volume covered by the primary X-ray beam. At depth x, the area of the primary beam equals $A_0(F + x/F)^2$ as obtained from the inverse square law.

Accurate use of the saturated-scatter method requires that the central axis depth–doses $D(x)$ have been measured using a field area large enough that conditions of saturated scatter exist at the central axis. The field A_0 used in the actual irradiation may be much smaller than that needed to determine the depth doses $D(x)$ in Eq. (4). The method may be explained as follows. Consider the case of a thin pencil beam incident on a laterally infinite phantom. Scattered photons escaping from the pencil beam will impart energy to the phantom outside the beam. When the phantom is irradiated with an extended beam including the pencil, the energy imparted to the phantom from photons escaping the pencil beam will be exactly compensated by the energy imparted to the latter volume by photons scattered into it (principle of reciprocity). Thus the integration over the primary beam volume in Eq. (4) corresponds to summing up the total energy imparted to the phantom (inside and outside the primary beam) from pencil beams evenly distributed over the entrance area A_0.

The saturated-scatter method was used or discussed by Meredith and Neary (1944), Bewley et al. (1959), Carlsson (1963) and Harrison (1983). Carlsson (1963) corrected saturated-scatter depth doses, obtained with a thick phantom, for the loss of backscattered photons before the data were applied to thinner phantoms. Harrison (1983) accounted for the lateral escape from finite sized patients by using central axis depth doses from a $30 \times 30\,\mathrm{cm}^2$ field for adult patients and for a $20 \times 20\,\mathrm{cm}^2$ field for paediatric patients. Conversion factors ε/KAP derived by Harrison (1983) tend to overestimate the energy imparted as compared to Monte Carlo calculations by 6–18% (Shrimpton and Wall, 1983).

3.2.2. Measurements using KAP meters

3.2.2.1. Calibration of the chamber to measure $\int_A K_{\mathrm{c,air}}\,\mathrm{d}A$. The calibration of the chambers should be performed such that the chamber measurement indicates the radiation incident on the patient and not on the chamber. Since the chamber attenuates about 15% (Larsson et al., 1998) of the incident X-rays, a corresponding error in clinical patient measurements will be introduced if the chamber is calibrated for the X-ray beam incident on it.

The chambers are normally calibrated mounted on the tube housing, in the position used for patient measurements. The reference ion chamber, with a calibration factor traceable to a primary standard, is

[1] In these measurements the statistical fluctuations in the interaction processes are generally not noticeable, being much smaller than other uncertainties in the measurements. Therefore, in Section 3, bars denoting expectation values are sometimes excluded. Quantities like energy fluence, Ψ, and kerma, K, are by definition expectation values (ICRU, 1980) and in equations where these quantities occur, expectation bars are used.

placed on the central axis (NRPB, 1992). Problems with the calibration arise due to the inhomogeneity of the X-ray beam caused by the heel effect, extrafocal radiation, secondary radiation generated in the collimators, tube housing and the chamber itself.

A protocol for the calibration procedure has been published by NRPB (1992). This protocol recommends that the chamber be calibrated for each individual X-ray stand in a geometry where the reference chamber is positioned at 100 cm focal distance and irradiated at the center of a $10 \times 10\,cm^2$ field. The calibration constant is calculated as the quotient between the product $K_{c,air} \cdot A_{nom}$ and the signal Q from the chamber (corrected as appropriate for factors such as temperature and atmospheric pressure). The nominal beam area, A_{nom}, is determined as the area within 50% of the maximum optical density on a film exposed in a standard screen cassette, irradiated at the position of the reference chamber and perpendicular to the X-ray beam. The beam area should be determined with an uncertainty of no more than 5% at the 95% confidence level, for a beam area of $100\,cm^2$. The recommendations given in IEC 580 IEC (1977) state that the maximum optical density used in the measurements should be below OD = 0.5. Shrimpton and Wall (1982) and, later, Faulkner et al. (1992) reported an overall uncertainty of $\pm 6\%$ at the 95% confidence limit for this calibration method.

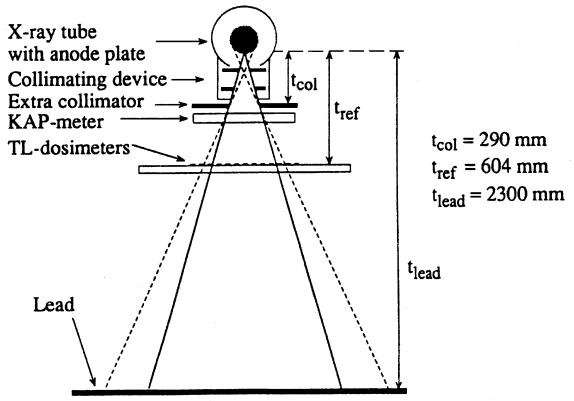

Fig. 1. The experimental set-up for determination of air-collision kerma integrated over beam area A, $\int_A K_{c,air}\,dA$. A 3 mm thick square lead collimator is placed close to the plane-parallel ionization chamber (KAP meter) and defines the area of the KAP meter irradiated. TL dosimeters (TLD) are placed perpendicular to the beam axis. For absolute determination of $K_{c,air}$ on the reference axis, the TLDs are replaced by a spherical reference ionization chamber centred on the beam axis. The solid and dotted lines indicate the focal and extrafocal radiations, respectively. [Figure taken from Larsson et al. (1996) and reproduced with permission from IOP Publishing.]

Larsson et al. (1996) used a modified approach for the calibration of KAP meters giving an uncertainty in the calibration values of $\pm 3\%$ at the 95% confidence level. The principle of the calibration is demonstrated in Fig. 1.

The signal Q from the KAP meter is due to photons passing through its sensitive volume. These comprise (1) primary X-rays passing within the nominal beam area A_{nom} as well as (2) extrafocal radiation and photons scattered in the collimators and tube housing. To account for this, air kerma should be measured over the entire plane perpendicular to the beam axis. In Fig. 1, this was achieved by evenly distributing 400 LiF dosemeters within and outside the nominal beam area, A_{nom}. The calibration constant for the KAP meter was derived as

$$k = \int_A K_{c,air}\,dA/Q \tag{5}$$

where $\int_A K_{c,air}\,dA$ was obtained by summing the measured $K_{c,air}$ values from all 400 dosimeters. The measurements showed that the extrafocal radiation outside the nominal beam area contributed 4% to the total integral.

In the following, $\int_A K_{c,air}\,dA$ is called the KAP value (or just KAP). The calibration constant k obtained in this way is expected to be independent of the calibration geometry, i.e. of the actual distance between the KAP meter and the reference chamber (assuming the attenuation of the X-rays between the KAP meter and the reference chamber to be negligible). On the contrary, calibration constants k_s obtained from the simplified calibration (Shrimpton and Wall, 1982; NRPB, 1992)

$$k_s = \frac{K_{c,air,ref} \cdot A_{nom}}{Q} \tag{6}$$

depend on the calibration geometry.

Fig. 2 shows results of a comparison of calibration constants, k_s, determined using the simplified method (cf. Eq. (6)) under different conditions by different practitioners in Sweden. Fig. 2 shows the values of k_s normalised to the calibration constant k using the Larsson method (cf. Eq. (5)). The calibration factors show variations of $\pm 20\%$; 90% of the calibration factors being within $\pm 10\%$. The deviation between the results is mainly caused by the different sizes of the nominal beam area used in the calibrations.

The energy dependence of the calibration constant is shown in Fig. 3 for two types of KAP meter. Both are built of PMMA plates but different types of conducting layers are used. The chamber with the smallest energy dependence (upper curve) has conducting layers of graphite. The other chamber (Diamentor) has conducting layers containing tin. The photo-

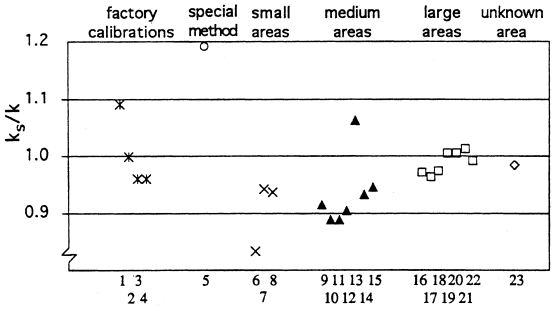

Fig. 2. The quotient k_s/k of the calibration constant k_s (simplified method) as determined at different hospitals and X-ray installations and k (Larsson method). Tube potential 90–120 kV. (*) factory calibration, (○) special calibration. Data points for which the calibration beam is known are divided into three groups: (×) small area $<80\,cm^2$, (▲) medium area 80–120 cm^2 and (□) large area $>120\,cm^2$. Diamond: area unknown. [Figure taken from Larsson et al. (1998) and reproduced with permission from IOP Publishing.]

electrons liberated in the tin contribute to an increased sensitivity of the chamber and cause an increased energy dependence.

With an undercouch installation, the X-ray beam is attenuated by the table top before reaching the patient. This needs to be considered by lowering the value of the calibration constant in proportion to the attenuation in the couch, typically about 20%.

Manufacturers often provide KAP meters with a single calibration factor representing all tube potentials and an average for under- and overcouch installations. This introduces an additional uncertainty in the recorded KAP-values which adds to the uncertainty from the primary calibration (cf. Fig. 2). NRPB (1992) recommends that the total uncertainty in recorded

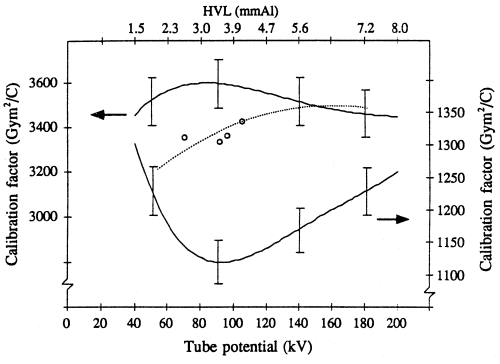

Fig. 3. Calibration factors for two KAP meters normalized to NTP. Lower solid curve (KAP meter 1, right ordinate), upper solid curve (KAP meter 2, left ordinate). The dotted line and symbol (○) were taken from Carlsson (1965) (KAP meter 2). The error bars indicate ± 2 combined standard uncertainties (3%). [Figure taken from Larsson et al. (1996) and reproduced with permission from IOP Publishing.]

KAP values for patient dose measurements should remain ≤25% at the 95% confidence level. For dedicated applications, e.g. for optimization of diagnostic procedures, higher demands on the uncertainty may be required. The above cited results from KAP meter calibrations indicate that with careful calibration and correcting for known influence factors, it should be possible to register KAP-values with an overall uncertainty of ±5%.

3.2.2.2. Conversion of the chamber reading to energy imparted to the patient. The chamber reading Q is related to the KAP value by means of the calibration factor k. The KAP value $= kQ$ can be converted into the radiant energy, R_{in}, incident on the patient. This requires knowledge of the X-ray energy spectrum, the energy fluence Ψ of the incident photons and the mass energy absorption coefficient of air $(\mu_{en}/\rho)_{air}$

$$\begin{aligned}\bar{R}_{in} &= \int_A \Psi \cos\theta \cdot dA = \int_A \frac{K_{c,air}\, dA}{(\overline{\overline{\mu_{en}/\rho}})_{air}} \cos\theta \cdot dA \\ &= \frac{1}{(\overline{\overline{\mu_{en}/\rho}})_{air}} \cdot \int_A K_{c,air} \cos\theta \cdot dA \\ &= \frac{\overline{\cos\theta}}{(\overline{\overline{\mu_{en}/\rho}})_{air})} \cdot \int_A K_{c,air}\, dA \end{aligned} \quad (7)$$

Here, $(\overline{\mu_{en}/\rho})_{air}$ is the mass energy absorption coefficient averaged over the photon energy spectrum at area element dA; $(\overline{\overline{\mu_{en}/\rho}})_{air}$ is further averaged over the area elements of the total beam and θ is the angle of incidence to the normal of area element dA. The bar used in $\bar{R}_{in}$ indicates that expectation values are considered in the equation (see footnote [1]).

Usually, the approximation $(\overline{\cos\theta}) \approx 1$ can be used and R_{in} be obtained from

$$R_{in} = \frac{k \cdot Q}{(\overline{\overline{\mu_{en}/\rho}})_{air}} \quad (8)$$

Normally, averaging of the mass energy absorption coefficient, Eq. (8), is only performed with respect to the energy spectrum of photons on the central axis, the averaging over beam area being neglected. Energy spectra of X-rays emitted at different emission angles from the anode and extrafocal radiation have been measured by, for example, Svahn (1977) and were taken into account by Larsson et al. (1996) in calibrating the LiF dosemeters (Fig. 1) used to measure air collision kerma.

In order to derive the energy imparted to the patient, the radiant energy escaping from the patient, R_{out}, must also be determined. Pychlau and Bunde (1965) used a man-shaped phantom and a thick NaI spectrometer placed at more than 400 points around the phantom to derive R_{out}. Carlsson (1963) used Monte Carlo calculated backscattered energy fractions

from the literature (Berger and Raso, 1960) and derived the transmitted radiant energy from depth doses determined with saturated scatter. The values of R_{out} can finally be used to calculate the conversion between measured values of R_{in} and ε

$$\bar{\varepsilon} = \bar{R}_{in} - \bar{R}_{out} = \bar{R}_{in}\frac{\bar{R}_{in} - \bar{R}_{out}}{\bar{R}_{in}} = \bar{R}_{in} \cdot \mathrm{IF} \quad (9)$$

where IF is the imparted fraction = the fraction of the radiant energy incident on the patient that is imparted to it. (The bars in Eq. (9) indicate that expectation values are used to derive values of IF, being a non-stochastic quantity.)

Finally, the factor that converts the measured KAP value to the energy imparted can be obtained by combining Eqs. (8) and (9):

$$\frac{\bar{\varepsilon}}{k \cdot Q} = \frac{\bar{\varepsilon}}{\mathrm{KAP}} = a \cdot \mathrm{IF} \cdot \frac{1}{(\overline{\overline{\mu_{en}/\rho}})_{air}} \quad (10)$$

where a denotes the fraction of the incident beam that actually hits the patient (Jones and Wall, 1985). The energy in the fraction $(1-a)$ of the beam, that passes outside the body may be included in calculating the imparted fraction. In this case, the imparted fraction $\mathrm{IF}_t < \mathrm{IF}$ multiplies R_{in} in the entire beam (Shrimpton et al., 1984). When using imparted fractions from the literature, it is important to combine them with the correct value of the incident radiant energy. Imparted fractions are nowadays preferably calculated using Monte Carlo techniques (see Section 3.3). Using this method, as well as when using the methods reviewed above, extrafocal radiations are not considered. Extrafocal radiation passing outside the nominal beam area, may or may not hit the patient. The details of the spatial distribution and energies of this radiation are in general not known. However, they need to be investigated before values of imparted fractions can be corrected to include the energy imparted to the patient from this source of radiation.

3.3. Use of Monte Carlo techniques for estimating energy imparted to the patient

3.3.1. The Monte Carlo method

The Monte Carlo computational method has found extensive application for the estimation of energy imparted to both patient and image receptor. It is necessary to estimate energy imparted in many different situations where it may not be practicable to make measurements. The Monte Carlo approach allows considerable flexibility and the possibility of varying both the X-ray imaging system and the model of the patient as required.

The Monte Carlo methodology requires a model of the imaging system and patient and knowledge of the relevant photon and electron interactions. Fig. 4 shows a simple model of both the imaging system and patient, taken from Sandborg et al. (1994a). In this case the patient is treated as a homogenous block of tissue. The X-ray field size may be varied as required and the phantom size altered to simulate patients of different ages or weights, or partial-body irradiations such as mammography. The X-ray spectrum may also be altered and the inclusion of grid and image receptor facilitates calculation of energy imparted to the receptor.

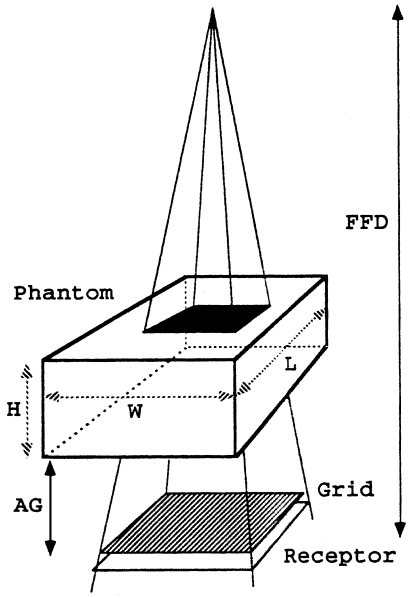

Fig. 4. The irradiation geometry showing phantom dimensions (length, L; width, W; thickness, H), the entrance field area (upper black area), air gap length, AG, and focus-receptor distance, FFD. The striped area shows the location of the anti-scatter grid, just above the image receptor. [Figure taken from Sandborg et al. (1994a) and reproduced with permission from Elsevier Scientific Publishers Ireland.]

The Monte Carlo technique works by simulating the histories of individual photons, (Morin, 1988), following them through the patient and imaging system and recording all energy deposited. At each stage in this process, the appropriate photon parameters are sampled in accordance with the known probability distribution functions. For the model illustrated in Fig. 4, photon histories start at the focal spot of the X-ray tube where the photon energy is selected using the specified X-ray spectrum and the photon direction chosen to lie within the required radiation field. Photons are traced to the entrance surface of the slab and the contribution to the entrance air kerma at this surface (without back-scatter) calculated. The photon is then traced into the slab where it may or may not interact. The photon interactions allowed in the slab are photo-

electric absorption, coherent and incoherent scatter and the choice between them is made in accordance with the magnitude of the relevant interaction cross sections. For the photon energies used in diagnostic radiology, it is normal to assume that any electrons produced are locally absorbed. The energy of the photoelectron and any Auger electrons liberated as a result of photoelectric interactions in the phantom therefore contribute directly to the energy imparted. Characteristic X-rays may also be emitted following the photoelectric absorption, but for the low atomic number materials in human tissue materials, their emission probability is low and they are of low energy and short range. Once again they can be assumed to be locally absorbed. The same is not true for photoelectric absorption in the image receptor, where characteristic X-rays are emitted with high probability and carry off an appreciable fraction of the photon energy. For gadolinium, the probability of emission of a K-fluorescent photon following a K-shell event is 0.93 and the average energy of the K-fluorescent X-ray is 43.9 keV. Such energetic photons are not locally absorbed and their histories are followed as part of the Monte Carlo simulation.

There is also energy transfer to an electron for incoherent scattering, but none for coherent scattering, where the photons change direction, but not energy. However, the energy transfer to recoil electrons for incoherent scattering can be quite small. The transfer is greatest when the initial photon is scattered backwards and is then 5.4, 11.4 and 28.1 keV for photon energies of 40, 60 and 100 keV, respectively.

If the photon does interact in the slab and the interaction simulated is photoelectric absorption, the history is terminated. If, however, the interaction is a scattering process, the new scatter direction is selected and the photon history continued. In this way the photon is followed until it leaves the slab or is absorbed. Photons may also pass straight through the slab without interacting. By following many photon histories, estimates can be made of the energy imparted to the slab, the imparted fraction (IF); the incident air kerma without backscatter and hence of the kerma area product (KAP) and the conversion factor (ε/KAP).

If the grid and image receptor are included in the model, the simulation can be extended so that an estimate of the energy imparted to the receptor can also be made. This is particularly valuable as it facilitates the estimation of relative values of energy imparted to the phantom for different imaging situations. This of course needs an assumption about the requirements for the energy imparted per unit area of the receptor. For screen-film imaging, this value is usually assumed to be a constant.

Because of the stochastic nature of the Monte Carlo computation process, there is a statistical error associated with all estimated quantities, which decreases inversely as the square root of the number of photon histories. It is important therefore to ensure that sufficient photon histories are followed. In some situations, this can require extended computational time and various computational devices may be employed to reduce the variance (Morin, 1988; Sandborg et al., 1994a).

3.3.2. Results from Monte Carlo computations

Imparted fractions and conversion factors for relating KAP readings to energy imparted in simple phantoms have been calculated by many authors. Shrimpton et al. (1981, 1984) used cylindrical phantoms with elliptical, rectangular (20 cm × 30 cm) or circular cross sections to simulate the trunk. Field sizes were defined at the mid-plane of the phantom and were 5, 20 and 30 cm square for AP projections and 10 and 20 cm square for lateral projections. For the smaller field sizes the X-ray beam was positioned at several locations across the phantom. The focus-skin distance and the filtration and waveform of the X-ray set were also varied. Fig. 5 shows their results for the imparted fraction as a function of tube potential. The error bars indicate the spread of values obtained as the model parameters were altered as described above. The results show a variation of no more than ±10%.

Fig. 5 also shows the results obtained by Shrimpton *et al.* for X-ray examinations of the head. In this case they used an inhomogeneous mathematical phantom developed at NRPB to estimate the imparted fraction for AP, PA and lateral projections at fixed field sizes. The error bars indicate a spread of ±3% arising from the differences in projection and beam filtration. The field size covered the entire head and was not varied. The lower IF values for the head, only 60% of those

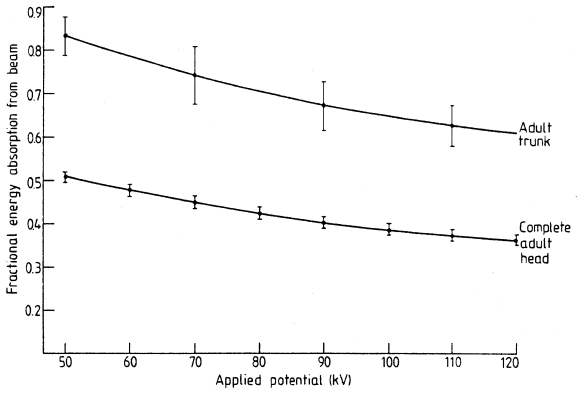

Fig. 5. Variation of the imparted fraction with applied tube potential of an adult anthropomorphic phantom during simulations of the trunk and the entire head. [Figure taken from Shrimpton et al. (1984) and reproduced with permission from IOP Publishing.]

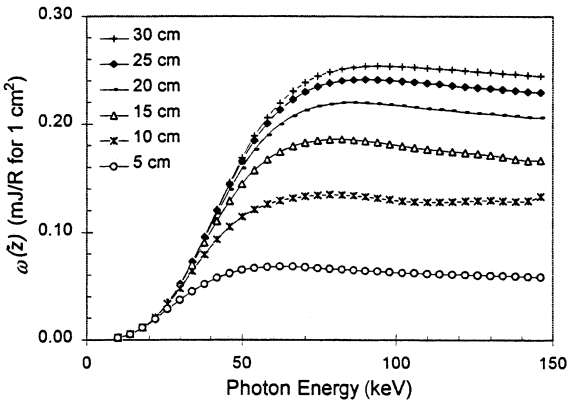

Fig. 6. The energy imparted per unit kerma-area product, $\omega(Z)$, as a function of photon energy of monoenergetic photons for water phantoms with thicknesses from 5 to 30 cm. [Figure taken from Gkanatsios and Huda (1997) and reproduced with permission from American Institute of Physics.]

for the trunk, were obtained since 37% of the beam was estimated to pass directly outside the head, whereas 100% of the field hits the trunk. The IF-values presented by Shrimpton *et al.* are thus for the entire beam (IF = IF_t). Shrimpton *et al.* estimate that the likely variations of field size and shape used in practice would produce a variation in the IF values of less than $\pm 15\%$.

Persliden and Alm Carlsson (1984) have calculated imparted fractions for laterally infinite phantoms for both monoenergetic photons and for X-ray spectra. Similar work has been done by Gkanatsios and Huda (1997) who have estimated KAP to energy imparted conversion factors using laterally infinite phantoms. Their calculations are for a 1 cm^2 square field incident on phantoms of thickness 5–30 cm in steps of 5 cm, for monoenergetic photons and for tube potentials of 60–140 kV in steps of 20 kV. Their work included a study of the effect of added filtration, voltage ripple and target angle. They found that for fixed tube potential and half value layer, the influence of target angle and ripple was small, producing only a 2% change in the conversion factor. Fig. 6 shows the dependence of their calculations of the KAP to energy imparted conversion factor on photon energy and phantom thickness. For each thickness the imparted fraction reaches a plateau energy, above which it changes very little.

The calculations of Alm Carlsson et al. (1984) were made for both laterally infinite and laterally finite water slabs. Their results are presented as conversion factors for laterally infinite slabs and correction factors which relate the imparted fractions for a finite slab to that for an infinite slab. They found that the conversion factors for the adult trunk were fairly independent of projection (AP or lateral). The greater thickness in the lateral projection being compensated by the smaller breadth, which allows greater escape of energy through the walls of the phantom. Fig. 7 shows their results comparing the imparted fraction for a laterally infinite slab to that for a finite rectangular slab in AP and lateral projections. The results in Fig. 7(a) are for a 40 kV spectrum (HVL 1.5 mm Al) and show that the imparted fraction for the finite slab is close to that for the laterally infinite slab. This is because of the small mean free path for such low energy X-rays. Larger differences are shown by their results at 130 kV (HVL 5.00 mm Al), Fig. 7(b). In the AP projections there is a fall off of IF/IF_∞ with increasing field size, which reaches 10% at the largest field size investigated and a focus film distance of 1000 mm. In the lateral projection the increased energy escape through the walls of the phantom causes a larger decrease in the quotient IF/IF_∞ with increasing field size.

Persliden and Sandborg (1993) have calculated the conversion factor $\bar{\varepsilon}$/KAP for a series of slab phantoms representing children. The phantoms comprise ICRU soft tissue (ICRU, 1980) and are of varying dimensions

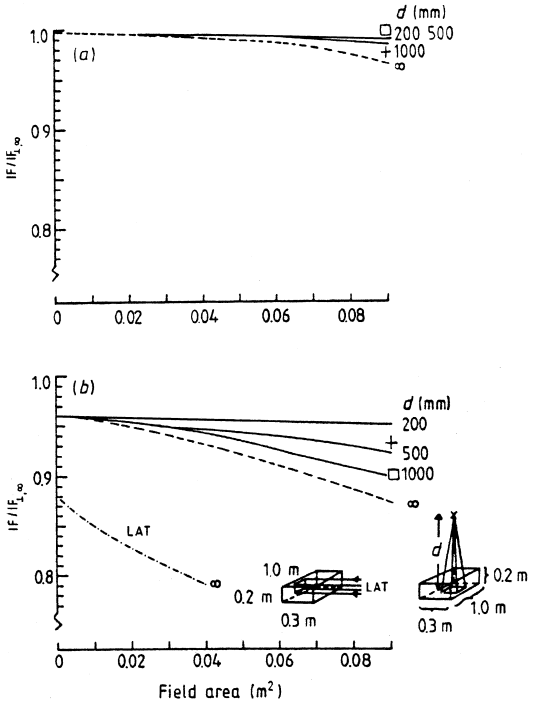

Fig. 7. The imparted fraction (IF) for a laterally finite water slab (dimensions and geometry shown) normalised to IF_∞ for a laterally infinite slab of the same thickness and perpendicular incidence as a function of field (quadratic) area with focal distance d as a parameter. (a) 40 kV, HVL = 1.5 mm Al; (b) 130 kV, HVL = 5.0 mm Al. Values for 100 mm (+), 300 mm (□) thick slabs for d = 1000 mm and the largest field area are included. – · –, IF/IF_∞ for $d = \infty$ and lateral (LAT) irradiation. [Figure taken from Alm Carlsson et al. (1984) and reproduced with permission from IOP Publishing.]

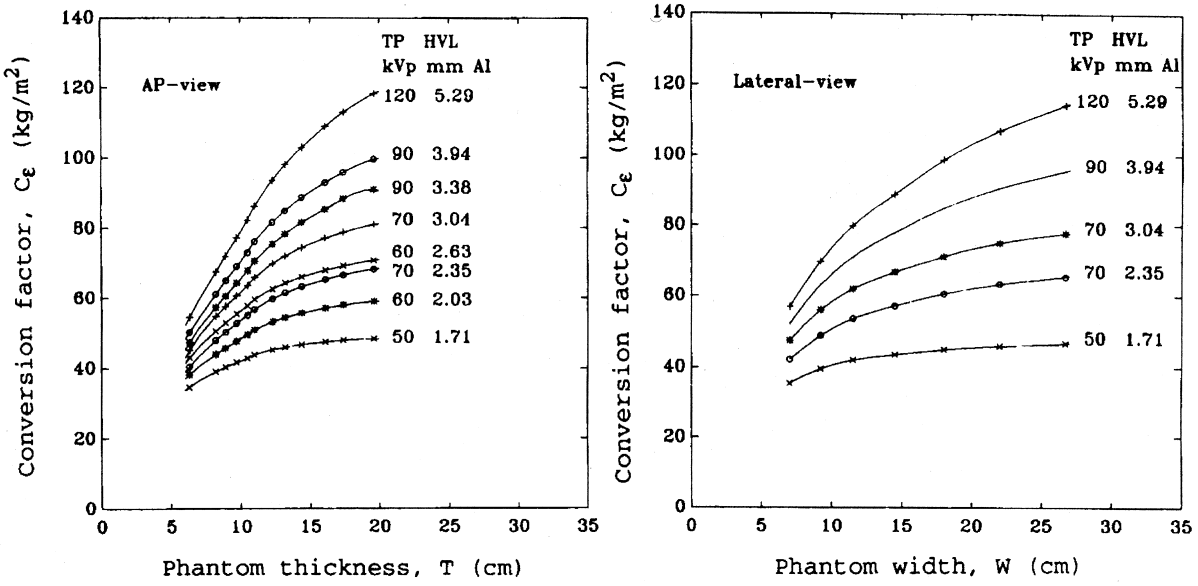

Fig. 8. Conversion factor between the energy imparted to the phantom and the entrance air collision kerma integrated over beam area as a function of phantom thickness in (a) AP view and (b) lateral view. The different curves show the variation with energy spectrum. Numbers included in the figure denote tube potential (TP, in kVp) and half-value layers, HVL (mm Al). [Figure taken from Persliden and Sandborg (1993) and reproduced with permission from Munksgaard International Publishers.]

representing a neonate, a new born child and children aged 6 months, 3, 10 and 15 a. The choice of dimensions was based on data from Swedish health care centres and ICRP report 23 (ICRP, 1974). The phantom sizes vary from $6.3 \times 7.0 \times 13.8\ cm^3$ (neonate) to $19.6 \times 26.7 \times 48.6\ cm^3$ (15 a old child). Fig. 8 shows how the conversion factor varies with the phantom thickness in AP and lateral projections. The conversion factor in both cases is for a radiation field extending across the full width of the phantom. Fig. 8 shows that the conversion factor increases as expected with increasing phantom thickness and photon energy. For the same phantom thickness in the direction of the beam, the conversion factor is smaller in the lateral than the AP projection. Conversion factors for neonates have also been calculated by Chapple et al. (1994), using a laterally infinite slab 5 cm thick. Their results are in good agreement with the results of both Shrimpton et al. (1984) and Persliden and Sandborg (1993).

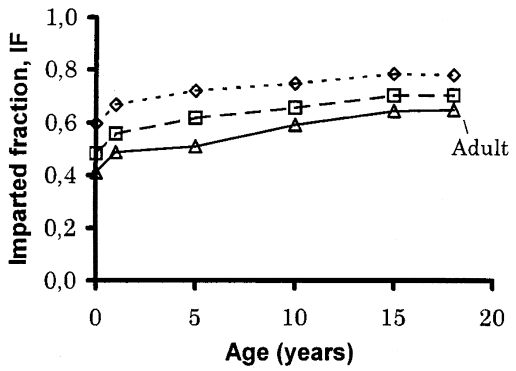

Fig. 9. Variation of imparted fraction, IF, with age of the patient for different tube potentials: ◇: 60 kV, □: 80 kV and △: 100 kV. The data for an adult is plotted at 18 years. [Data taken from Hart et al. (1994) and Hart et al. (1996)].

The above calculations were made for simple homogenous phantoms, but it is also possible to make the calculations using more complicated phantoms which better represent the human anatomy. Hart et al. (1994) and Hart et al. (1996) provide values of the imparted fraction for a wide range of X-ray examinations, X-ray spectra and both adult (1994) and child (1996) anthropomorphic phantoms. The data are available as software reports. Fig. 9 shows values of their imparted fraction for the chest PA examination at three tube potentials. The imparted fraction increases slowly with increasing phantom size because of the accompanying increase in the field size for the examination. As demonstrated previously, there is a stronger dependence on tube potential as higher energy photons have a greater probability of escaping the phantom.

Gibbs et al. (1987) used an anthropomorphic phantom derived from CT images of a female cadaver to calculate organ absorbed doses in intra-oral radiography. Values of IF derived from their calculations are shown in Fig. 10, taken from the work of Carlsson and Alm Carlsson (1990). IF-values for an adult math-

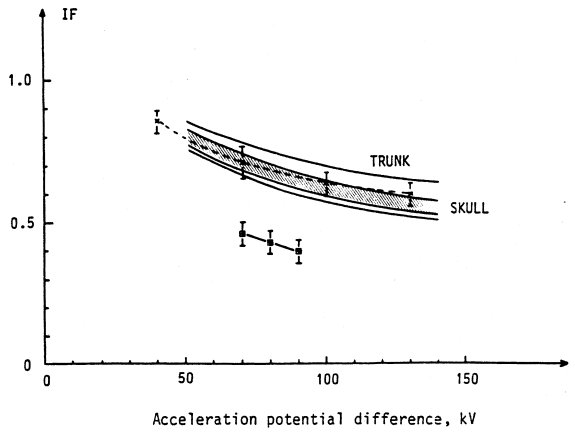

Fig. 10. Ranges of IF values in irradiations of the trunk and entire skull (shaded area), derived using Monte Carlo calculations and a mathematical (adult) phantom in simulating 12 common X-ray examinations (Jones and Wall, 1985). The variation in IF for each tube potential (acceleration potential difference) is due to variations in beam geometry and beam filtering. Values of IF are also given for (×) a 150 mm thick, laterally infinite water slab with indicated ranges due to an extreme variation in beam filtering (Alm Carlsson et al., 1984) and (■) periapical dental radiography derived for a female patient with indicated ranges due to variations in projection only (Gibbs, 1988, personal communication). [Figure taken from Carlsson and Alm Carlsson (1990) and reproduced with permission from Academic Press.]

ematical phantom and 12 common X-ray examinations of the trunk and skull, calculated by Jones and Wall (1985), are also shown. The IF values for the intra-oral projections are considerably lower than those for the trunk and skull due to the comparatively thin body parts irradiated in intra-oral examinations. The error bars indicate variations due to the projection. The ranges given for the trunk and skull (the entire skull being irradiated in all projections) correspond to variations in both projection and beam filtration. Also included in Fig. 10 are IF-values calculated by Alm Carlsson et al. (1984) for a 150 mm thick, laterally infinite water slab. The error bars indicate variations in beam quality due to an extreme variation in beam filtering. The results show that the IF values for a 150 mm thick laterally infinite water slab provide good approximations to the mid range values of IF for both trunk and skull. In Fig. 10, the IF values are valid for the part of the beam that actually hits the patient, contrary to the IF values in Fig. 5 which were derived for the entire beam allowing for radiation passing outside the body.

Fig. 11, also taken from the work of Carlsson and Alm Carlsson (1990), shows values of the conversion factor ε/KAP obtained when the imparted fractions from Fig. 10 and constant-potential-energy spectra from Birch et al. (1979) are used. The conversion factor increases rapidly with increasing tube potential and half value thickness (HVT). At low tube potentials (<70 kV), the conversion factor depends on both tube potential and HVT, the rapid variation with HVT being due to the strong energy dependence of $(\mu_{en}/\rho)_{air}$ (cf. Eq. (10)). The error bars show the variations due to the different projections used in the examinations.

The energy imparted from specialised X-ray examinations has also been estimated using Monte Carlo techniques. Dance (1980) calculated the energy imparted to cylindrical phantoms representing the breast and has derived incident air kerma to mean breast dose conversion factors. More complicated breast models have been used by various authors (e.g. Rosenstein et al., 1985; Dance, 1990; Wu et al., 1991; Zoetelief and Jansen, 1995) to calculate the energy imparted to particular regions of the breast for estimation of mean glandular dose. A detailed discussion of this topic is given in Dance et al. (1998).

Atherton and Huda (1995) used the EGS4 code to simulate CT examinations and calculated the energy imparted to circular phantoms. They divided the energy imparted into contributions arising from absorption of primary and secondary photons and studied phantom diameters of 160 and 320 mm. A wide range of phantom compositions were studied including lung and bone. Fig. 12 shows how the imparted fraction varies with the mass of material in the CT slice. Huda et al. (1997) used the EGS4 code with right elliptical cylinders to simulate head and body CT examinations. The tissue density and phantom dimensions were varied to simulate neonates, children aged 1, 5, 10 and 15 years and an adult. The energy imparted per slice per unit axial dose was calculated and used as a basis for the estimation of effective dose.

It was noted previously that models which also calculate the energy imparted to the image receptor can be used to predict the dependence of energy imparted to the patient or patient dose on various system parameters. An example of this type of application is the work of Sandborg et al. (1994b) on the design of antiscatter grids and choice of tube potentials for various X-ray exams. This paper calculated the energy imparted to a rectangular slab simulating the patient for fixed energy imparted per unit area of the image receptor. The resulting energy imparted to the patient was used as a cost function when comparing different designs of grid and different tube potentials. Fig. 13 shows an example of the results. Image quality is kept constant while the lead strip widths are varied at three different strip frequencies. The optimal strip width is obtained when the mean absorbed dose in the phantom ($\bar{D}=\bar{\varepsilon}/M$) takes its minimum value.

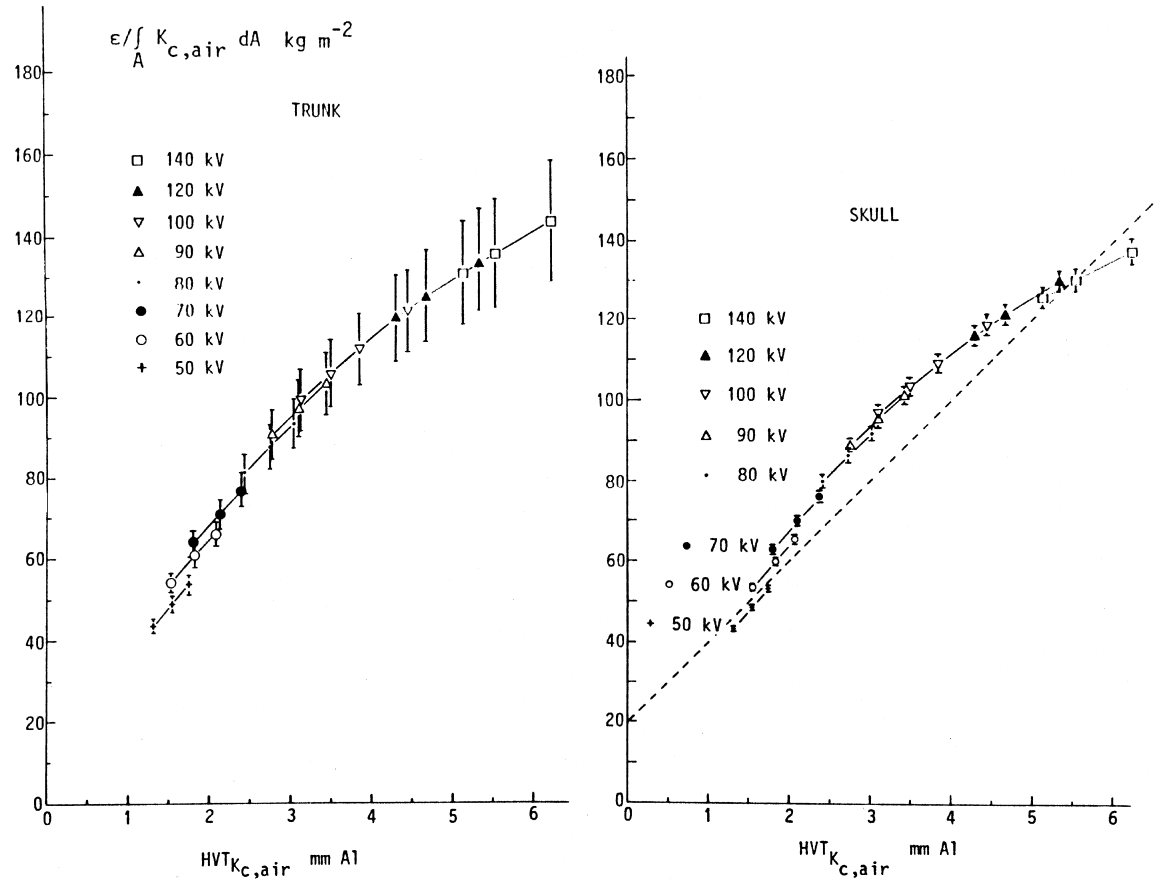

Fig. 11. Conversion factor, $\varepsilon/\int_A K_{c,air}\,dA$ as a function of the half-value thickness (HVT) with the tube potential as parameter for examinations of the adult trunk (left) and adult skull (right). The values were derived using IF values from Jones and Wall (1985) and constant-potential-energy spectra from Birch et al. (1979). It is assumed that the entire beam hits the patient. The dashed, straight-line approximation (right) was used by Stenström and Karlsson (1988) for tube potential <70 kV and intraoral radiography. [Figure taken from Carlsson and Alm Carlsson (1990) and reproduced with permission from Academic Press.]

3.4. The energy imparted to the patient as a risk indicator

Stochastic risks from irradiation of organs/ body tissues are at present considered to be related to the spatial mean of absorbed dose in the organs, $\bar{D}_T$, rather than to the energy imparted to them (ICRP, 1991). By definition, $\bar{D}_T = \bar{\varepsilon}_T/m_T$, where m_T is the mass of organ T. This relation is used in deriving values of $\bar{D}_T$ from, for example, Monte Carlo simulations and demonstrates the basic importance of the concept of energy imparted. The effective dose E (ICRP, 1991) is a quantity that is intended to be proportional to the detriment to a population due to stochastic effects and is based on the concept of equivalent dose H_T:

$$H_T = \sum_R w_R \cdot \bar{D}_{T,R}$$

where w_R is the radiation weighting factor which takes into account the relative effects of radiation quality on risk. For X-rays used in diagnostic radiology, it is assumed that $w_R = 1$ (see, however, Brenner, 1989).

Although defined for a population of radiation workers, effective dose has been extensively used to estimate patient risks in X-ray diagnostic examinations. To take into account the age distribution of patients, the risk per unit of effective dose may be reduced to about 60% of that for radiation workers (Kaul et al., 1997). If paediatric patients are considered it should probably be increased.

Patient doses are increasingly expressed as organ or effective doses (ICRP, 1991) and measured KAP-values are converted directly using E/KAP factors instead of ε/KAP factors. To be able to interpret earlier measurements of energy imparted to the patient in terms of effective dose, the relation between E and ε needs to be established (Section 3.4.1). Situations also exist where such conversions are very uncertain and the energy

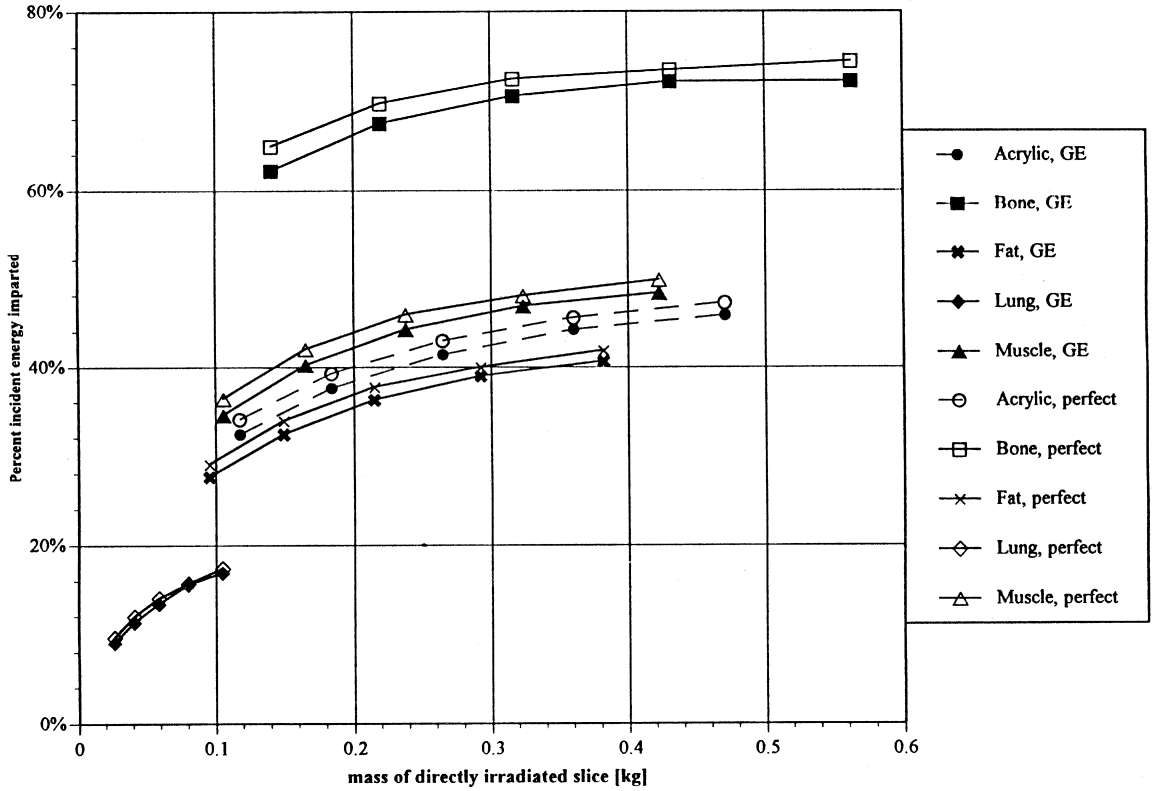

Fig. 12. The imparted fraction as a function of the mass of the directly irradiated phantom for 80 keV photons and a CT slice thickness of 5 mm. [Figure taken from Atherton and Huda (1995) and reproduced with permission from IOP Publishing.]

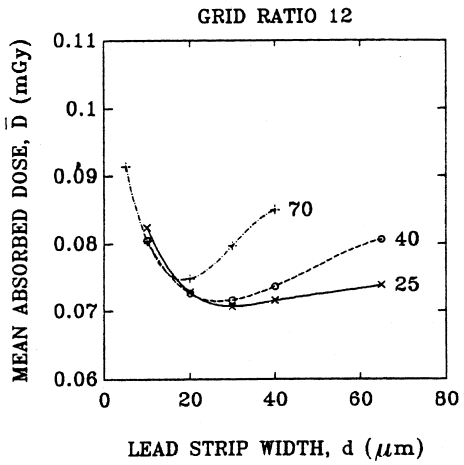

Fig. 13. The mean absorbed dose, $\bar{D}=\bar{\varepsilon}/M$, in the soft tissue phantom, representing a lumbar spine examination in AP view as a function of the lead strip width, d, of the anti-scatter grid. Grids with ratio 12 and lead strip frequencies 25, 40 and 70 cm^{-1}. The tube potential is adjusted so that the contrast of a 1 mm bone detail is 3%. [Figure taken from Sandborg et al. (1994b) and reproduced with permission from British Institute of Radiology].

imparted may remain a practical quantity of choice for risk estimations (Section 3.4.2). To indicate levels of risk encountered in X-ray diagnostic examinations, a review of estimated risks per unit energy imparted are given in Section 3.4.3.

3.4.1. The relation between energy imparted and effective dose

The energy imparted to the patient is, by itself, not a good estimate of risk. For instance, if 1 J is imparted to a 70 kg adult and a 10 kg child, the risk will be quite different in the two cases (disregarding the higher risks related to a child per unit of effective dose). If the body is homogeneously irradiated such that $\varepsilon = 1$ J, the effective doses for the adult and the child are 14 and 100 mSv/J, respectively.

In many situations, the mean absorbed dose $\bar{D}=\bar{\varepsilon}/M$, where M is the total body mass, provides a reasonable estimate of effective dose and hence of risk. Both quantities are weighted averages of the mean organ doses $\bar{D}_T$ although with different weighting factors, Eqs. (11) and (12) (Alm Carlsson and Carlsson, 1986):

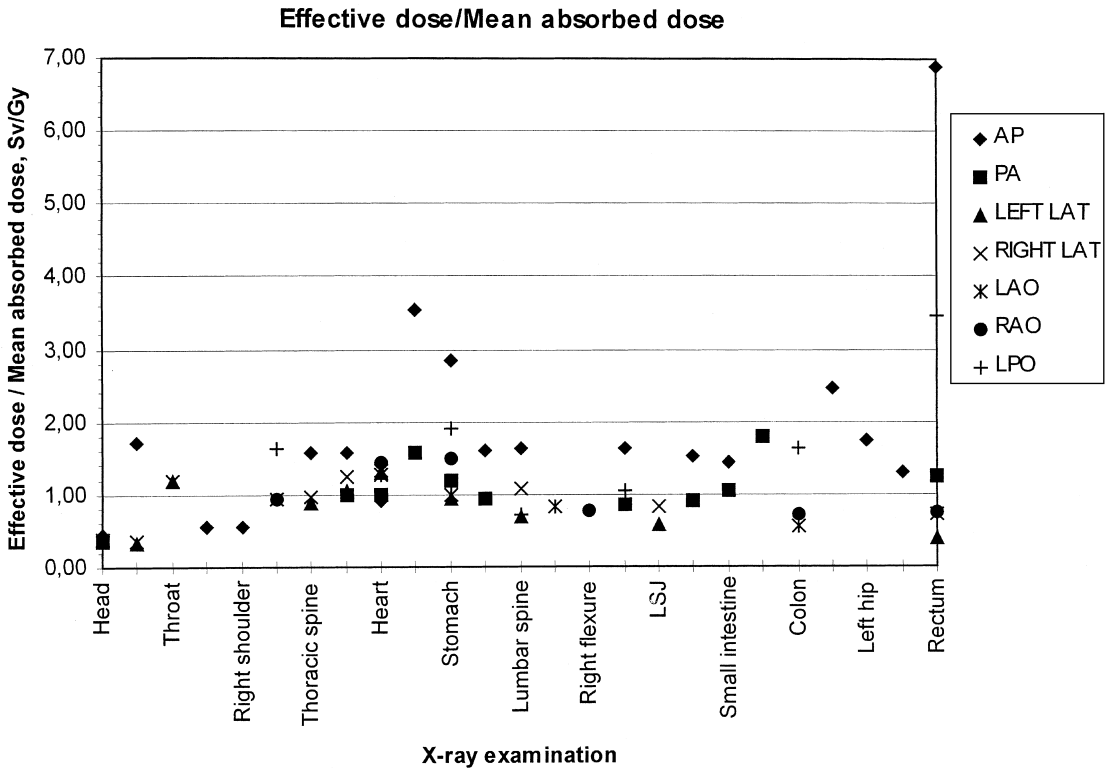

Fig. 14. The quotient of effective dose E and mean absorbed dose in the body $\bar{D}$ for X-ray examinations of the trunk and head as indicated on the axis. The view is parameter. AP: anterior posterior, LAT: lateral, LPA: left posterior oblique, LAO: left anterior oblique, RAO: right posterior oblique. Data are taken from Table 1 in Huda and Gkanatsios (1997).

$$\bar{D} = \frac{\bar{\varepsilon}}{M} = \frac{\int_M D \, \mathrm{d}m}{M} = \sum_T \bar{D}_T \cdot \frac{m_T}{M}; \quad \sum_T \frac{m_T}{M} = 1 \qquad (11)$$

$$E = \sum_T w_T \cdot H_T; \quad \sum_T w_T = 1 \qquad (12)$$

Here, the tissue weighting factors w_T give the relative risk from organ T in a homogeneous whole body irradiation while the weighting factors for $\bar{D}_T$ are the relative masses (m_T/M) of the organs. It follows that for a homogeneous whole body irradiation, or if the body is assumed to contain a uniform mixture of the organs, $E = \bar{D}$. The deviation of $E/\bar{D}$ from unity is a measure of the inhomogeneity of the irradiation.

Recently, Huda and Gkanatsios (1997) derived values of the quotient E/ε between effective dose and energy imparted to a 70.9 kg phantom using data from Hart et al. (1994) for 68 projections as function of beam quality (tube potentials 50–120 kV). Their results are shown in Fig. 14, represented as values of $E/\bar{D}(\bar{D} = \bar{\varepsilon}/M$; M = 70.9 kg). Fig. 14 shows that most of the values balance around unity within a factor of two (0.5–2.0 Sv/Gy). The highest values are identified for examinations with a radiosensitive organ at shallow depths in the X-ray beam, e.g. the gonads in the rectum AP view ($E/\bar{D} = 6.8$). Correspondingly, values below unity indicate that radiosensitive organs are protected by overlaying tissues or that the most radiosensitive organs are situated outside the primary beam. The data also show that in most cases $E/\bar{D}$ increases with increasing tube potential and, for each projection, asymptotically approaches a constant value indicating that the relative depth doses in the body get increasingly more uniform. On the contrary, in the rectum AP view, $E/\bar{D}$ decreases with increasing photon energies since the gonad dose decreases relative to that of the other organs. In most cases, the variation with tube potential is small, the largest variation occurring in the head AP view where $E/\bar{D}$ increases by a factor of two in going from 50 to 120 kV (3.0 mm Al total filtration). There is also a small but significant dependence on beam filtration.

The equivalent dose to the breasts at mammography is typically 1–2 mSv yielding an effective dose of 0.05–0.10 mSv. The tissue weighting factor for the breast is a mean for men and women, with approximately zero risk for men. In this situation, it will be more useful to note the mean organ dose and derive the risk using the

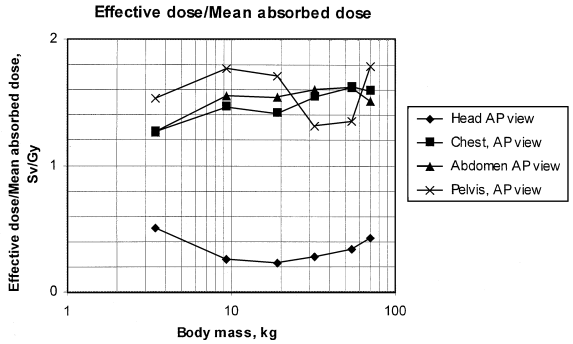

Fig. 15. The quotient of effective dose E and mean absorbed dose in the body $\bar{D}$ as a function of body mass (paediatric and adult phantoms) for pelvis AP, ×; abdomen AP, ▲; chest AP, ■ and head AP, ◆. Data are taken from Fig. 3 in Huda and Gkanatsios (1997).

specific risk coefficient (risk/organ dose) for that organ.

Huda and Gkanatsios (1997) also derived values of E/ε for differently sized paediatric phantoms using data from Hart et al. (1996). Fig. 15 shows the corresponding quotients $E/\bar{D}$ for 4 examinations as function of the body mass. As shown in Fig. 15, $E/\bar{D}$ is fairly independent of the body mass, but varies with examination and view. There is, however, need for more investigations on the variation of $E/\bar{D}$ with patient dimension, field size and position. Tapiovaara et al. (1997) have developed a Monte Carlo program with a size and sex adjustable phantom which may be useful in future research on this topic.

3.4.2. Special situations

The tabulated data used (Hart et al., 1994, 1996) to convert KAP-values to values of E are generally valid for a standardized geometry with fixed field sizes and positions. Using other field sizes and positions, the conversion factors E/KAP may vary considerably.

Gosch and Gursky (1992) showed that large variations in organ doses may occur due to a slight repositioning of the incident X-ray field (±5 cm caudally and cranially from a central position). In a kidney examination, the lung dose was found to vary by a factor of 18. The authors concluded that in complex examinations involving fluoroscopy, where field size, field position and tube potential vary during the course of the examination, energy imparted to the patient may be the best risk related quantity to use.

When small body volumes are irradiated as in intra-oral radiography, considerable uncertainties arise due to difficulties in selecting the organs to be included into the "remainder" and because the remainder contributes a dominant fraction to E, as much as 80% in intra-oral examinations (Stenström et al., 1987; Gibbs, 1989). Stenström *et al.* concluded that the energy imparted should be preferred for risk estimates. For similar reasons, Huda and Atherton (1995), advocate use of the energy imparted in CT examinations. Leitz et al. (1995) adopted essentially the same point of view in assessing the risk from CT examinations. In these calculations, the authors mixed the organs of the trunk into one single organ that was given the weighting factor 0.9, while the neck and head were given weighting factors 0.05 and 0.04, respectively.

The examples discussed above show that the energy imparted to the patient is still a useful quantity for practical use. It also has the attractive feature of being a physical quantity that does not vary with time. Since more than 50% of the atomic bomb survivors are still alive, the tissue weighting factors are likely to be changed in the future and values of effective doses recalculated.

3.4.3. Examples of estimated risk per unit of energy imparted

Bengtsson et al. (1978) estimated from a study of patient exposures in Sweden that the risk for long-term effects was $2 \times 10^{-4}\,J^{-1}$ (within a factor of 2 up or down) disregarding sex or age. The estimate was based on KAP- and organ dose measurements/calculations from 15 different X-ray examinations in 13 hospitals. The organ risk factors used were based on data given by ICRP (1977).

In Report 53 from The Institute of Physical Sciences in Medicine, (Wall et al., 1988) it is argued that in appropriate circumstances (complex examinations) the use of energy imparted provides a practical approach for estimating the risk to patients. A risk vs energy imparted correlation exists for several common X-ray examinations as were performed in England, based on measurements from 20 hospitals. The risk factor for fatal cancers and serious hereditary defects from the first two generations was estimated to be $2.3 \times 10^{-4}\,J^{-1}$. For a uniform whole body irradiation (mass = 70.9 kg) this corresponded to $1.63 \times 10^{-2}\,Sv^{-1}$, in close agreement with the risk factor published in 1977 by ICRP of $1.65 \times 10^{-2}\,Sv^{-1}$. This number ($1.65 \times 10^{-2}\,Sv^{-1}$) is today believed to be $5 \times 10^{-2}\,Sv^{-1}$ (ICRP, 1991), a factor of approximately 3 times larger as estimated from an extended follow up of the atomic bomb survivors. Huda (1984) gives risk factors for fatal cancers, non-fatal cancers and hereditary effects for male and female in CT examinations. Risk factors are given for head-, chest-, abdomen- and pelvis scans and are 6×10^{-4}, 9.5×10^{-4}, 11.2×10^{-4} and $18.5 \times 10^{-4}\,J^{-1}$, respectively. These values are much larger than those given by Bengtsson et al. (1978) and Wall et al. (1988). This is due inclusion of both non-fatal cancers and hereditary effects of all future generations by Huda. Also, Bengtsson et al.

(1978) reduced the genetic risk component by taking into account the child expectancy of a typical population. The energy imparted to an adult varies considerably depending on the type of examination. Typical values range from 0.1 mJ [one bite-wing film in intra-oral radiography (Stenström et al., 1986)] to 1000 mJ [barium enema examination (Wall et al., 1988)].

Both values of energy imparted and risk coefficients are expected to change with time due to technical developments, examination protocols and extended follow up of the atomic bomb survivors.

4. Application to image receptors

The image receptor absorbs X-rays leaving the patient and records the information in the radiation beam to form the image. This in turn provides information to the radiologist. The accuracy and precision by which the information is conveyed depends on the performance of the receptor. The first step in the chain of processes determining overall performance is the impartation of energy to the receptor volume.

The requirements on receptor performance are several and partly conflicting. A receptor should have *high sensitivity* to keep patient doses low, *sufficient sharpness* to detect small details and separate between details lying close together and *low noise* to enable high accuracy in differentiating between tissues of similar X-ray absorption properties. Many image receptors must be made thin to limit the lateral spreading of the signal carriers so that a high inherent receptor sharpness is maintained. The fraction of absorbed X-rays will be accordingly low. To increase sensitivity, the receptors are often made from high atomic number elements with an increased probability for photo-electric absorption, particularly at energies just above the K-absorption edge. Escape of the concomitantly emitted characteristic X-rays contributes to increased noise. Alternatively, the sensitivity of a screen-film system can be increased by increasing its light conversion efficiency. However, this also increases the noise since the energy imparted to the screen, and consequently the number of photons interacting, for equal light emission (i.e. film blackening) is reduced. In Fig. 16, the absorption properties (attenuation coefficients) of the rare-earth screens Gd_2O_2S and LaOBr are compared with $CaWO_4$; for a long time period (since the discovery of the X-rays) the most used material in fluorescent screens. The rare-earth screens are attractive due to their increased absorption probabilities compared to $CaWO_4$ for a wide range of photon energies used in general radiography (due to the positions of their K-absorption edges) and higher light conversion efficiencies. Fig. 16 also shows for comparison the attenuation

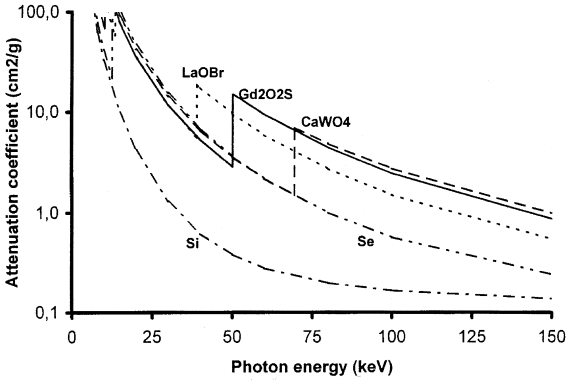

Fig. 16. The dependence with photon energy of the mass attenuation coefficient of LaOBr, Gd_2O_2S and $CaWO_4$ phosphor materials and for semi-conductor materials Si and Se. The discontinuities at 12.7, 38.9, 50.2 and 69.5 keV are due to the K-absorption edge in the high-Z elements, Se, La, Gd and W, respectively.

coefficients for the semiconductor materials Si and Se which are used in some digital systems. The energy imparted to the receptor can be derived from the number and size of energy impartation events taking place in its volume. An event is here due to the interaction of an incident photon and its associated secondary particles (electrons, characteristic X-rays). The number of events is Poisson distributed and the energy imparted in an event is given by the energy of the interacting photon minus the energies of the associated secondary particles which escape from the receptor volume. The receptor characteristics (sensitivity, contrast, sharpness and noise) depend on the details of these processes which themselves are suitably calculated using the Monte Carlo method as described in Section 3.3.1. In the following, the significance of the concept of energy imparted to the image receptor is elucidated and effects on image quality and patient dose are discussed.

4.1. Sensitivity

Shuping and Judy (1977) and Kodera et al. (1984) found that the energy imparted to a fluorescent screen per unit area, needed to obtain a certain optical density on the film, was independent of the energy spectrum of the incident X-rays. Shuping and Judy determined the energy imparted to the screen experimentally by measuring the difference in the energy fluence of incident and exiting photons (using a Ge spectrometer) and correcting for fluorescent escape from the screen. Kodera *et al.* used Monte Carlo techniques to estimate the imparted fractions from primary and scattered photons exiting a water phantom positioned in front of the screen. Vyborny (1976), however,

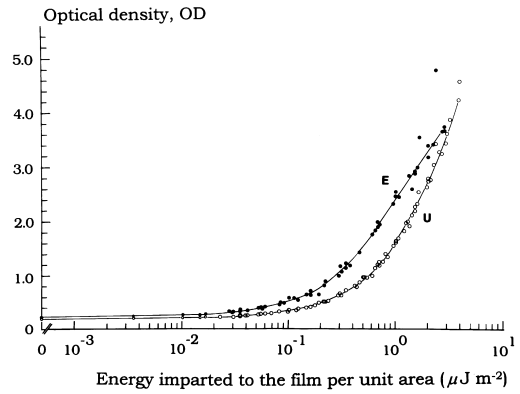

Fig. 17. The film characteristic (H and D) curve for dental X-ray films: optical density as a function of the energy imparted to the film per unit area for Kodak Ultraspeed (○) and Kodak Ektaspeed (●) films and for different tube potentials 36, 47, 59 and 77 kV. [Figure taken from Helmrot et al. (1991) and reproduced with permission from Butterworth-Heinemann.]

reported that to obtain a certain film optical density at photon energies below 30 keV, the energy imparted per unit area of the screen had to be increased. Photons of low energies interact close to the entrance surface of the screen (far from the film emulsion) and the emitted light photons have an increased probability of absorption before reaching the film. Except for mammography, the photons transmitted through the patient and incident on the screen with energies below 30 keV are few in number. However, obliquely incident scattered photons may also impart energy at shallow depths in the screen. The cited experiments show that the light transmitted to the film of a screen-film system is approximately proportional to the energy imparted to the screen. Corrections to direct proportionality may be needed in some cases.

For dental (direct) X-ray films, Helmrot et al. (1991) found that there exists a unique relationship between the net optical density on the film and the energy imparted per unit area, $d\varepsilon/dA$, to the AgBr grains of the film emulsion. This is shown in Fig. 17. In calculating $d\varepsilon/dA = D\cdot(dm/dA)$ where dm/dA is the mass of AgBr per unit area of the film emulsion, it was assumed that D equals the collision kerma, $K_{c,AgBr}$, in AgBr.

The above findings justify the assumption that relative sensitivities of different image receptors can be derived theoretically from their energy absorption properties (Holje, 1983). This assumption is useful in deriving theoretical models of the imaging chain based on transport (Monte Carlo) calculations (Sandborg et al., 1994a).

The sensitivity of fluorescent screens is often expressed as the inverse of the air kerma, K_{air} at the screen needed to obtain a film net optical density of 1.0. The sensitivity expressed in this way varies in proportion to $\bar{\varepsilon}_{det}/K_{air}$ where $\bar{\varepsilon}_{det}$ is the expectation value of the energy imparted to the receptor per unit area. When the photons are perpendicularly incident on the screen $\bar{\varepsilon}_{det}/K_{air}$ is proportional to $IF_{det}/(\overline{\mu_{en}/\rho})_{air}$ which is shown in Fig. 18(a) for three screens of different phosphor materials (IF_{det} = the fraction of energy incident on the detector that is imparted). The rapid increase in sensitivity at low photon energies is due to the rapid decrease of $(\overline{\mu_{en}/\rho})_{air}$ with increasing photon energy. Holje (1983) defined the sensitivity as the inverse of the energy fluence Ψ of photons incident on the receptor, which is required to produce net optical density 1.0. The sensitivity then varies in proportion to IF_{det} which is shown in Fig. 18(b). The latter way of defining the sensitivity gives values for the sensitivity which are directly related to the energy imparted to the screen and facilitates understanding of the behaviour of the receptor in an X-ray field.

4.2. Derivation of image quality descriptors

The variation of optical density on an X-ray film is due to differing attenuation of the X-rays passing through the various structures of the body. The contrast due to the attenuation difference between rays passing beside and through a contrasting detail is the most fundamental parameter of physical image quality. All kinds of noise limit the accuracy with which a given contrast can be detected. When the incident X-rays impart energy to the receptor, the contrast in the incident beam is modified and this is described in Section 4.2.1. The noise due to the statistical variations in the energy imparted to the receptor is discussed in Section 4.2.2.

4.2.1. Contrast

The object contrast C obtained in capturing the image at the receptor, is given by

$$C = \frac{E(\varepsilon_{p,1}) - E(\varepsilon_{p,2})}{E(\varepsilon_{p,1})} \cdot \frac{1}{1 + E(\varepsilon_s)/E(\varepsilon_{p,1})} = C_p \cdot \frac{1}{1 + S/P} \quad (13)$$

where $E(\varepsilon_{p,1})$, $E(\varepsilon_{p,2})$ and $E(\varepsilon_s)$ are the expectation values of the energies imparted to the receptor per unit area by primary photons beside the detail, subscript (p, 1), in the shadow of the detail, subscript (p, 2) and by scattered photons, subscript (s). The ratio $E(\varepsilon_s)/E(\varepsilon_{p,1})$ is usually called the scatter-to-primary ratio, S/P.

When the photons incident on the image receptor are monoenergetic, contrast C can also be calculated using simply the fluence Φ of photons incident on the receptor instead of the energy imparted. This holds

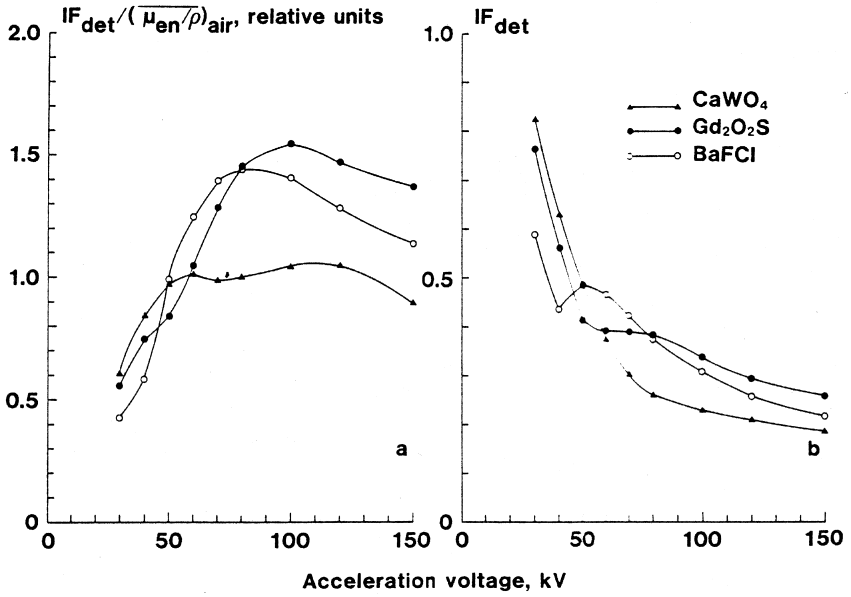

Fig. 18. The energy dependence of the sensitivity of fluorescent screens defined in terms of the reciprocal of (a) the exposure and (b) the energy fluence needed to obtain a given film optical density (energy imparted per unit area). Perpendicularly incident photons (primary photons filtered by 200 mm water) are assumed and imparted fractions in the receptor, IF_{det} are derived for $CaWO_4$, BaFCl and Gd_2O_2S screens of thickness 100 mg/cm^2 by means of Monte Carlo simulation. [Figure taken from Carlsson and Alm Carlsson (1990) and reproduced with permission from Academic Press.]

since there exists a direct proportionality between the energy imparted to the receptor per unit area and the fluence Φ. When the incident X-rays are distributed in energy, it is no longer sufficient to use the fluence to calculate the contrast. This was emphasized by Wagner (1977) in analysing the imaging properties of rare-earth screens. He introduced the concept of "intrinsic screen contrast" or "contrast rendition factor" as a measure of the effect on contrast of the conversion of radiant energy in the incident beam to energy imparted to the receptor. The intrinsic screen contrast was defined as the ratio between the primary contrast C_p, as defined in Eq. (13) and the primary "radiation contrast" $C_{p,\Psi}$ obtained by replacing the energy imparted per unit area beside and behind the detail with the corresponding values of the energy fluence. The intrinsic screen contrast was calculated for 200 μm thick screens of different fluorescent materials and normalised to the intrinsic contrast of a (Zn, Cd)S:Ag screen. The results show that the intrinsic contrast decreases from 0.94 for a Y_2O_2S:Tb screen to 0.71 for a Gd_2O_2S screen when imaging an 1 mm thick bone detail within 150 mm of water using 100 kV X-rays.

Scattered photons reaching the image receptor degrade contrast (Eq. (13)). The influence of scatter on contrast can be deduced from values of scatter fractions F, defined by $F = S/(P + S)$, which are obtainable from experiments (Stargardt and Angerstein, 1975; Dick et al., 1978). Kalender (1981) used Monte Carlo simulations to derive scatter fractions using screens of different thicknesses and atomic compositions. The energy imparted was used in the response function for the receptors. Kalender found that values of the scatter fractions depended on the receptor encountered in the measurements. For instance, the scatter fractions for X-rays transmitted through a 10 cm water slab, irradiated with a 10 × 10 cm^2 field of 40 and 120 keV incident photons are 39 and 31%, respectively, using a totally absorbing receptor but 39 and 48% using a 60 mg cm^{-2} CsI detector. This was an important finding and Kalender was able to resolve conflicting results from measurements of scatter fractions in the literature.

It is now standard practice to use the energy imparted to the receptor in calculating values of contrast and S/P ratios (see, for example, Dance and Day, 1984; Nielsen and Carlsson, 1984; Alm Carlsson et al., 1986; Sandborg et al., 1994a).

4.2.2. Quantum noise

Screen-film systems require a given energy imparted per unit area to produce a given optical density and contrast is probably the most relevant image quality descriptor. Digital systems allow image processing and image contrast can be manipulated in the displayed image. In this case, the limiting noise contribution will be that from statistical fluctuations in the energy imparted to the receptor (quantum noise). Patient

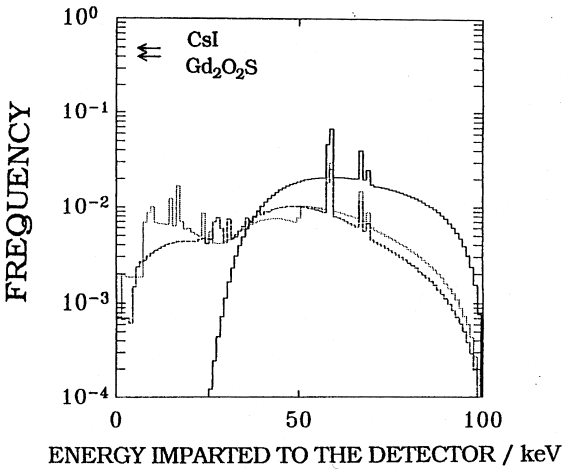

Fig. 19. The frequency function of energy impartation events of perpendicularly-incident primary photons as a function of event size (energy imparted to the receptor) for photons generated at 100 kV tube potential, with total filtration of 2.5 mm Al and transmitted through 200 mm water. Totally absorbing receptor, ———; 100 mg/cm^2 CsI, - - - and 140 mg/cm^2 Gd_2O_2S, · · ·. The arrows in the upper left corner mark the probabilities of zero impartation events. [Figure taken from Sandborg and Alm Carlsson (1992) and reproduced with permission from IOP Publishing Ltd.]

absorbed dose may then reach a minimum value which cannot be further reduced without loss of information. In digital systems, therefore, the most important image quality descriptor is the signal-to-noise ratio, SNR.

4.2.2.1. Single event distributions. The relative variance $V(\varepsilon)/E^2(\varepsilon)$ in the energy imparted ε to the receptor can be written (Sandborg and Alm Carlsson, 1992)

$$\frac{V(\varepsilon)}{E^2(\varepsilon)} = \frac{V(n)}{E^2(n)} + \frac{1}{E(n)} \cdot \frac{V(\lambda)}{E^2(\lambda)} = \frac{1}{E(n)} \cdot \frac{E(\lambda^2)}{E^2(\lambda)} \tag{14}$$

where $V(n)$ and $E(n)$ are the variance and mean (expectation value) of the number of photons incident on the receptor and λ is the energy imparted to the receptor by an incident photon and its associated secondary particles. The expectation values $E(\lambda)$ and $E(\lambda^2)$ are the first and second moments, respectively, of the energy imparted in a single event. The last equality follows from $V(n) = E(n)$ for a Poisson distributed variable and $V(\lambda) = E(\lambda^2) - E^2(\lambda)$. The first ($i = 1$) and the second ($i = 2$) moments are given by

$$E(\lambda^i) = \int_0^\infty \lambda^i f(\lambda)\, \mathrm{d}\lambda$$

where $f(\lambda)\,\mathrm{d}\lambda$, the single event distribution, is the probability that the energy imparted in an event falls in the interval λ, $\lambda + \mathrm{d}\lambda$. Fig. 19 shows the frequency function $f(\lambda)$ for CsI (100 mg/cm^2) and Gd_2O_2S (140 mg/cm^2) image receptors, taken from the work of Sandborg and Alm Carlsson (1992).

For the receptors shown in Fig. 19, there is a large probability of zero energy impartation events as indicated by the arrows in Fig. 19. These are due to photons transmitted through the receptor without interacting or photons interacting through coherent scattering before escaping. The low energy part of the single event distribution is mainly due to escaping K-photons, created in photoelectric absorptions in the receptor, giving rise to events with the energy imparted equal to $h\nu - E_K$, where $h\nu$ is the energy of the incident photon and E_K the energy of the K-photon. Photons interacting via Compton scattering, followed by escape of the scattered photons from the receptor volume, are rare and make a small contribution to the single event distribution.

4.2.2.2. Signal-to-noise ratio. The signal-to-noise ratio squared, SNR^2, is given by the inverse of the relative variance in Eq. (14) and can be recast in the form below (Sandborg and Alm Carlsson, 1992)

$$\mathrm{SNR}^2 = E(n) \cdot \frac{E^2(\lambda)}{E(\lambda^2)} = E(n) \cdot A_q \cdot I \tag{15}$$

Here, A_q is the fraction of incident photons which impart energy to the receptor (i.e. interact in the receptor with $\lambda > 0$; interactions with $\lambda = 0$ also occur due to coherent scatterings as described above).

In Eq. (15), $E(n) \cdot A_q$ is the number of photons that interact in the receptor. It follows that the factor I, referred to as the "statistical factor" by Chan and Doi (1984), is given by

$$I = \frac{1}{A_q} \cdot \frac{E^2(\lambda)}{E(\lambda^2)}$$

For monoenergetic photons and a totally absorbing receptor, both A_q and I are unity. The signal-to-noise ratio is then given by $\sqrt{E(n)}$ which is the signal- to noise ratio of the Poisson distributed incident photons. If the receptor remains totally absorbing ($A_q = 1$) but is irradiated with a beam of energy distributed X-rays, the single event distribution is simply the normalised energy fluence spectrum of the photons. The statistical factor is then less than unity implying that energy distributed photons introduce an additional noise compared to monoenergetic photons. If the receptor only partly absorbs the incident photons, the statistical factor decreases further due to the broadening of the single event distribution. Thus, partly absorbing receptors introduce additional noise compared to a totally absorbing receptor.

Chan and Doi (1984) calculated values of A_q and I using Monte Carlo simulations. Fig. 20 shows their results for screens of 100 mg/cm^2 $Ba_{0.75}Sr_{0.25}SO_4$,

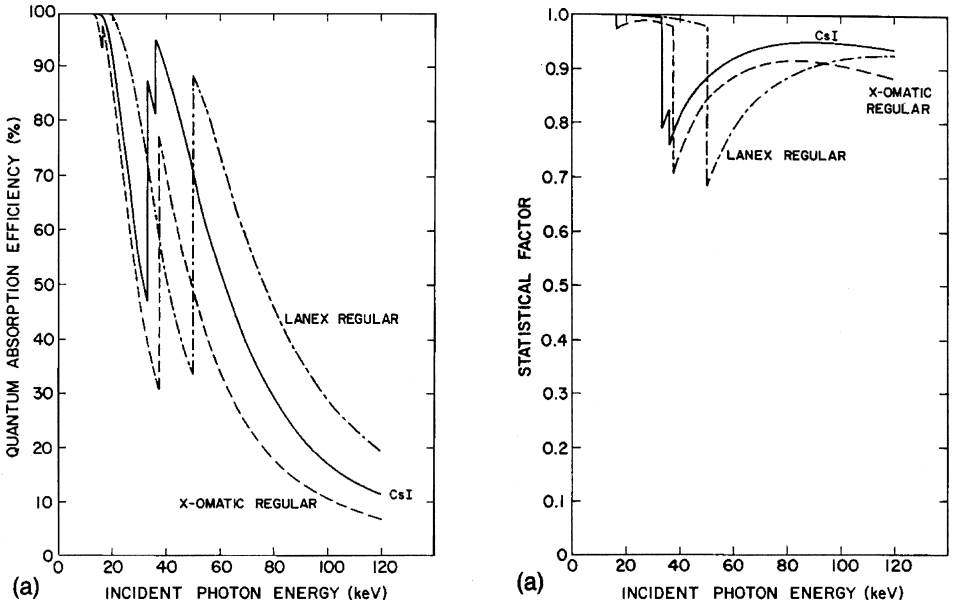

Fig. 20. The quantum absorption efficiency, A_q (a) and the statistical factor, I (b) as a function of photon energy for three different fluorescent screens and perpendicularly incident photons: 100 mg/cm^2 $Ba_{0.75}Sr_{0.25}SO_4$ (X-Omatic Regular), 140 mg/cm^2 Gd_2O_2S (Lanex Regular) and 100 mg/cm^2 CsI (X-ray image intensifier). [Figure taken from Chan and Doi (1984) and reproduced with permission from American Institute of Physics.]

140 mg/cm^2 Gd_2O_2S, and 100 mg/cm^2 CsI as a function of photon energy. Fig. 20 shows that A_q decreases with increasing photon energy but increases abruptly at the K-edge of the high-Z element(s) in the receptor due to the increased probability of photoelectric absorption. The factor I is close to unity below the K-edge as photo-electric absorption is the dominating interaction process and the photon imparts practically all its energy to the receptor (escape of characteristic L photons is negligible). Just above the K-edge, where the escape of K-fluorescent photons broadens the single-event distribution, I decreases to a minimum. At this energy, the K-photon carries away a large fraction of the incident photon's energy. This fraction decreases as the photon energy increases beyond the K-edge and I increases correspondingly.

The signal-to-noise ratio in Eq. (15) describes the relative fluctuations of energy imparted to pixel elements of a homogeneously irradiated receptor. When a contrasting detail is imaged, the detectability of the detail depends on the signal-to-noise ratio SNR_Δ as given by the signal relative to the noise in the background (Sandborg et al., 1994a):

$$SNR_\Delta^2 = \frac{|E(\lambda_1)E(n_{p,1}) - E(\lambda_2)E(n_{p,2})|^2}{[E(\lambda_1^2)E(n_{p,1}) - E(\lambda_s^2)E(n_s)]} \quad (16)$$

In Eq. (16), the signal in the numerator is given by the difference in the energy imparted to the receptor in the shadow area of the detail ($E(\lambda_i)E(n_{p,i}) = E(\varepsilon_{p,i})$), without ($i = 1$) and with ($i = 2$) the detail present; index s indicates corresponding values for the scattered photons (assumed to be independent of the presence of the detail). It is noted that the signal can be obtained from the product of the primary contrast, C_p, and $E(\varepsilon_{p,1})$, thus indicating the fundamental importance of the contrast.

Tapiovaara and Sandborg (1995) compared values of SNR_Δ as measured for circular PMMA (polymethyl-methacrylate) discs imaged on top of a PMMA phantom using a CsI image intensifier and calculated using Monte Carlo techniques. As shown in Fig. 21, the calculated values of the signal-to-noise ratio are in excellent agreement with the measured values down to a detail diameter of 3 mm. For smaller details, the effects of receptor unsharpness need to be taken into account. This example shows that calculations of the signal-to-noise ratio based on the energy imparted to the receptor represent an approximation which is very good for large area details. However, modifying factors such as the transport of the secondary information carriers and additional noise sources, need to be taken into account for small details (Swank, 1973; Nishikawa and Yaffe, 1990). In the example shown in Fig. 21, the calculated and measured SNR^2 values were slightly corrected (5%) to account for fluctuations in the light output.

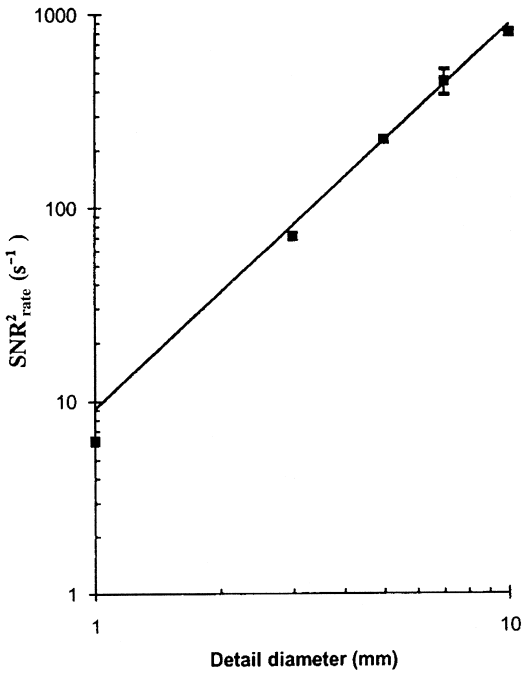

Fig. 21. SNR^2_{rate} for detecting a 3 mm thick PMMA disc detail, plotted as a function of the detail diameter. X-ray tube potential 51 kV, total filtration 22.7 mm Al, X-ray image intensifier input dose rate 0.153 μGy/s. Monte Carlo calculations assuming sharp system and white noise, ———; measurement, ■. [Figure taken from Tapiovaara and Sandborg (1995) and reproduced with permission from IOP Publishing Ltd.]

5. Concluding remarks

The energy imparted to the patient was the first quantity used in estimating stochastic risks from X-ray examinations. The use of the concept was closely associated with development of equipment, the KAP meter, for its measurement. Conversion of the KAP-meter readings are nowadays increasingly being expressed in terms of effective dose instead of energy imparted. The energy imparted to the patient is, however, still useful in practice, particularly when effective dose can only be determined with large uncertainty compared to energy imparted. This is the case in, for example, complex diagnostic procedures involving fluoroscopy, CT examinations and when small volumes are irradiated such as in intra-oral radiography. In the latter cases, problems arise in determining the effective dose due to the uncertainties in estimating the contribution to E from the remainder.

In clinical KAP meter measurements, large variations in registered values occur, to a great extent due to variations in patient size. The conversion of KAP values to energy imparted to the patients involves the use of imparted fractions, which, for adult patients, do not vary much with patient size. There will thus be a corresponding spread in values of energy imparted which will by themselves be badly related to risk. A better correlation to risk is obtained if energy imparted is normalized to patient mass, giving values of the mean absorbed dose $\bar{D} = \bar{\varepsilon}/M$ in the patient. As shown in Figs. 14 and 15, there exists a fairly close relationship between effective dose and mean absorbed dose, $\bar{D} = \bar{\varepsilon}/M$. The proportionality between these quantities depends on the projection and beam quality, with the largest deviations being due to projection. In a given X-ray examination, the projection may be sufficiently well known to allow a good choice of conversion between $\bar{D}$ and E.

The image receptor plays an important role for patient dose and image quality. The influence of the receptor on these parameters is to a first approximation well described by the energy imparted to the receptor. The energy imparted to the receptor is particularly useful for explaining the variations in patient dose and image quality due to variations in the X-ray energy spectrum. This is valuable in all work aiming at the optimisation of physical and technical parameters in X-ray examinations since an appropriate choice of X-ray energy spectrum (tube potential and filtration) is then a task of major importance.

Acknowledgement

The constructive criticism and suggestions by Professor Emeritus Carl A. Carlsson are gratefully acknowledged.

References

Alm Carlsson, G., Carlsson, C. A., Persliden, J., 1984. Energy imparted to the patient in diagnostic radiology: calculation of conversion factors for determining the energy imparted from measurements of the air collision kerma integrated over beam area. Phys. Med. Biol. 29, 1329–1341.

Alm Carlsson, G., 1985. Theoretical basis for dosimetry. In The Dosimetry of Ionizing Radiation, eds. K. R. Kase, B. E. Bjärngard and F. H. Attix, Vol. I, pp. 1–75. Academic Press, New York.

Alm Carlsson, G., Carlsson, C. A., 1986a. Relations between effective dose equivalent and mean absorbed dose (energy imparted) to patients in diagnostic radiology. Phys. Med. Biol. 31, 911–921.

Alm Carlsson, G., Carlsson, C. A., Nielsen, B., Persliden, J., 1986b. Generalised use of contrast degradation factors in diagnostic radiology. Application to vanishing contrast. Phys. Med. Biol. 31, 737–749.

Almén, A., Nilsson, M., 1996. Simple methods for determination of energy imparted, dose distribution and organ

doses in paediatric radiology. Phys. Med. Biol. 41, 1093–1105.

Atherton, J. V., Huda, W., 1995. CT doses in cylindrical phantoms. Phys. Med. Biol. 40, 891–911.

Bengtsson, G., Blomgren, P. G., Bergman, K., Åberg, L., 1978. Patient exposures and radiation risk in Swedish diagnostic radiology. Acta Radiol. Oncol. 17, 81–105.

Berger, M. J., Raso, D. J., 1960. Monte Carlo calculation of gamma-ray backscattering. Radiat. Res. 12, 20–37.

Bewley, D. K., Batchelor, A. L., Lowe, J., Nataadidjaja, E., Newbery, G. R., Opie, R., 1959. Integral doses at 200 kV and 8 MeV. Br. J. Radiol. 32, 36–46.

Birch, R., Marshall, B. and Adran, G. M., 1979. Catalogue of Spectral Data for Diagnostic X-rays. Scientific Report Series 30. The Hospital Physicists' Association, 47 Belgrave Square, London.

Boag, J. W., 1945. On the energy absorbed by a patient during X-ray treatment. Br. J. Radiol. 18, 235–238.

Brenner, D. J., 1989. Enhanced risk from low-energy screen-film mammography X-rays. Br. J. Radiol. 62, 910–914.

Carlsson, C. A., 1963. Determination of integral absorbed dose from exposure measurements. Acta Radiol. 1, 433–457.

Carlsson, C. A., 1965. Integral absorbed doses in roentgen diagnostic procedures. I. The dosemeter. Acta Radiol. 3, 311–325.

Carlsson, C. A. and Alm Carlsson, G., 1990. Dosimetry in diagnostic radiology and computerised tomography. In *The Dosimetry of Ionizing Radiation*, eds. K. R. Kase, B. E. Bjärngard and F. H. Attix, Vol. III, pp. 163–257. Academic Press, New York.

Chan, H. P., Doi, K., 1984. Studies of X-ray energy absorption and quantum noise properties of X-ray screens by use of Monte Carlo simulation. Med. Phys. 11, 37–46.

Chapple, C. L., Faulkner, K., Hunter, E. W., 1994. Energy imparted to neonates during X-ray examinations in a special care baby unit. Br. J. Radiol. 67, 366–370.

Cristy, M. and Eckerman, K. F., 1987. Specific Absorbed Dose Fractions of Energy at Various Ages from Internal Photon Sources. I. Methods. Report ORNL/TM-8381/VI. Oak Ridge National Laboratory, Oak Ridge, TN.

Dance, D. R., 1980. The Monte Carlo calculation of integral radiation dose in xeromammography. Phys. Med. Biol. 25, 25–37.

Dance, D. R., Day, G. J., 1984. The computation of scatter in mammography by Monte Carlo methods. Phys. Med. Biol. 29, 237–247.

Dance, D. R., 1990. Monte Carlo calculation of conversion factors for the estimation of mean glandular breast dose. Phys. Med. Biol. 35, 1211–1219.

Dance, D. R., Skinner, C. L. and Alm Carlsson, G., 1998. Breast dosimetry. Applied Radiation and Isotopes 50, 185–203.

Dick, C. E., Motz, J. W., 1981. Image information transfer properties of X-ray fluorescent screens. Med. Phys. 8, 337–376.

Dick, C. E., Soares, C. G., Motz, J. W., 1978. X-ray scatter data for diagnostic radiology. Phys. Med. Biol. 23, 1076–1085.

Faulkner, K., Busch, H. P., Cooney, P., Malone, J. F., Marshall, N. W., Rawlings, D. J., 1992. An international intercomparison of dose-area product meters. Radiat. Prot. Dosim. 43, 131–134.

Feddema, J. and Oosterkamp, W. J., 1953. Volume doses in diagnostic radiology. In *Modern Trends in Diagnostic Radiology*, ed. H. W. McLaren, 2nd series. Butterworth and Co., London.

Gibbs, S. J., 1989. Influence of organs in the ICRP's remainder on effective dose equivalent computed for diagnostic radiation exposures. Health Phys. 56, 515–520.

Gibbs, S. J., Pujol, A., Chen, T. S., Carlton, J. C., Dosmann, M. A., Malcolm, A. M., James, A. E., 1987. Radiation doses to sensitive organs from intraoral dental radiography. Dentomaxillofac. Radiol. 16, 67–77.

Gkanatsios, N. A., Huda, W., 1997. Computation of energy imparted in diagnostic radiology. Med. Phys. 24, 571–579.

Gosch, D., Gursky, S., 1992. Describing the radiation exposure of patients in diagnostic radiology on the basis of absorbed energy. Radiat. Prot. Dosim. 43, 115–117.

Happey, F., 1940. Volume integration of dosage for X- and γ-radiation. Nature (London) 143, 668–669.

Happey, F., 1941. The integration of radiation dosage and the absorption of energy in tissue for X- and gamma radiation. Br. J. Radiol. 14, 235.

Harrison, R. M., 1983. A re-evaluation of the "saturated scatter" method for estimating the energy imparted to patients during diagnostic radiology examinations. Phys. Med. Biol. 28, 701–707.

Hart, D., Jones, D. G. and Wall, B. F., 1994. Normalised Organ Doses for Medical X-ray Examinations calculated using Monte Carlo Techniques. NRPB (National Radiation Protection Board), NRPB-SR262, Oxon, U.K.

Hart, D., Jones. D. G. and Wall, B. F., 1996. Normalised Organ Doses for Paediatric X-ray Examinations calculated using Monte Carlo Techniques. NRPB (National Radiation Protection Board), NRPB-SR279, Oxon, U.K.

Helmrot, E., Alm Carlsson, G., Eckerdal, O., Sandborg, M., 1991. Influence of scattered radiation and tube potential on radiographic contrast: comparison of two different dental X-ray films. Dentomaxillofac. Radiol. 20, 135–146.

Helmrot, E., 1996. Systematic analysis of a radiological diagnostic system: A method for application in the effective use of X-rays in intraoral radiology. Thesis No. 498, Linköping University, Linköping, Sweden.

Henriksson, C. O., 1967. Iodine 125 as a radiation source for odontological roentgenology. *Acta Radiol.* Suppl. 269.

Holje, G., 1983. Physical properties of radiographic screen-film systems. Thesis, Lund University, Lund, Sweden.

Huda, W., 1984. Is energy imparted a good measure of the radiation risk associated with CT examinations? Phys. Med. Biol. 29, 1137–1142.

Huda, W., Atherton, J. A., 1995. Energy imparted in computed tomography. Med. Phys. 22, 1263–1269.

Huda, W., Atherton, J. V., Ware, D. E., Cumming, W. A., 1997. An approach for the estimation of effective radiation dose at CT in paediatric patients. Radiology 203, 417–422.

Huda, W., Gkanatsios, N. A., 1997. Effective dose and energy imparted in diagnostic radiology. Med. Phys. 24, 1311–1316.

International Atomic Energy Agency, IAEA, 1994. Proc. IAEA Int. Symp. on Measurement Assurance in Dosimetry, Vienna, 1993. IAEA, Vienna.

International Commission on Radiological Protection ICRP, 1974. Report of the Task group on Reference Man, ICRP Publication 23. Pergamon Press, Oxford.

International Commission on Radiological Protection ICRP, 1977. Recommendations of the International Commission on Radiological Protection, ICRP Publication 26. Pergamon Press, Oxford.

International Commission on Radiological Protection ICRP, 1991. 1990 Recommendations of the International Commission on Radiological Protection. *Annals of the ICRP*, Publication 60. Pergamon Press, Oxford.

International Commission on Radiation Units and Measurements ICRU, 1970. Linear Energy Transfer. ICRU Report 16. Washington, D.C.

International Commission on Radiation Units and Measurements ICRU, 1980. Radiation Quantities and Units. ICRU Report 33. Washington, D.C.

International Commission on Radiation Units and Measurements, ICRU, 1983. Microdosimetry. ICRU Report 36. Bethesda, MD.

International Electrotechnical Commission, IEC., 1977. Area Exposure Product Meters Standard. IEC 580.

Jones, D. J. and Wall, B. F., 1985. Organ Doses from Medical X-ray Examinations calculated using Monte Carlo Techniques. NRPB (National Radiation Protection Board), NRPB-R186, Oxon, U.K.

Kalender, W., 1981. Monte Carlo calculations of X-ray scatter data for diagnostic radiology. Phys. Med. Biol. 26, 835–849.

Kaul, A., Bauer, B., Bernhardt, J., Nosske, D., Veit, R., 1997. Effective dose to the members of the public from diagnostic applications of ionizing radiation in Germany. Eur. Radiol. 7, 1127–1132.

Kellerer, A. M., 1985. Fundamentals of microdosimetry. In *The Dosimetry of Ionizing Radiation*. eds. K. R. Kase, B. E. Bjärngard, F. H. Attix, Vol. I, pp. 77–162. Academic Press, New York.

Kodera, Y., Doi, K., Chan, H. P., 1984. Absolute speeds of screen-film systems and their absorbed-energy constant. Radiology 151, 229–236.

Larsson, J. P., Persliden, J., Sandborg, M., Alm Carlsson, G., 1996. Transmission ionization chambers for measurements of air collision kerma integrated over beam area. Factors limiting the accuracy of calibration. Phys. Med. Biol. 41, 2381–2398.

Larsson, J. P., Persliden, J., Alm Carlsson, G., 1998. Ionization chambers for measuring air kerma integrated over beam area. Deviations in calibration values using simplified calibration methods. Phys. Med. Biol. 43, 599–607.

Leitz, W., Axelsson, B., Szendrö, G., 1995. Computed tomography dose assessment: A practical approach. Radiat. Prot. Dosim. 57, 337–380.

Mayneord, W. V., 1940. Energy absorption. Br. J. Radiol. 13, 235–247.

Mayneord, W. V., Clarkson, J. R., 1944a. Energy absorption. II. Integral dose when the whole body is irradiated. Br. J. Radiol. 17, 151–157.

Mayneord, W. V., Clarkson, J. R., 1944b. Energy absorption. II. Integral dose when the whole body is irradiated. Br. J. Radiol. 17, 177–182.

Mayneord, W. V. and Clarke, R. H., 1975. Carcinogenesis and radiation risk: A biomathematical reconnaissance. *Br. J. Radiol.* Suppl. 12.

Meredith, W. J., Neary, G. J., 1944. The production of isodose curves and the calculation of energy absorption from standard depth dose data. Br. J. Radiol. 17, 126.

Morin, R. L. (ed.), 1988. Monte Carlo Simulations in the Radiological Sciences, CRC Press, Boca Raton, Florida.

Motz, J. W., Danos, M., 1978. Image information content and patient exposure. Med. Phys. 5, 8–22.

Nielsen, B., Carlsson, C. A., 1984. Energy imparted to fluorescent screens from primary and scattered radiation. Variation with atomic composition and screen thickness. Phys. Med. Biol. 29, 315–328.

Nishikawa, R. M., Yaffe, M. J., 1990. Model of the spatial-frequency-dependent detective quantum efficiency of phosphor screens. Med. Phys. 17, 894–904.

National Radiation Protection Board, NRPB, 1992. National Protocol for Patient Dose Measurements in Diagnostic Radiology. Dosimetry Working Party of the Institute of Physical Sciences in Medicine, NRPB, Oxon.

Persliden, J., Alm Carlsson, G., 1984. Energy imparted to water slabs by photons in the energy range 5–300 keV. Calculations using a Monte Carlo photon transport model. Phys. Med. Biol. 29, 1075–1088.

Persliden, J., Sandborg, M., 1993. Conversion factors between energy imparted to the patient and air collision kerma integrated over beam area in pediatric radiology. Acta Radiol. 34, 92–98.

Pychlau, H., Pychlau, P., 1964. Ein Diagnostik-Dosimeter-Grundform und Abwandlung. Detsch Röentgenkongr, 1963. Beih. Fortshr. Röentgenstr. 100, 177–180.

Pychlau, P., Bunde, E., 1965. The absorption of X rays in a body equivalent phantom. Br. J. Radiol. 38, 875–877.

Reinsma, K., 1962. Dosimeters for X-ray Diagnosis (Dutch edn, 1960). Philips Technical Library, Eindhoven.

Rosenstein, M., Andersen, L. W. and Warner, G. G., 1985. Handbook of Glandular Tissue Doses in Mammography. HHS Publications FDA85-8239. CDRH, Rockville, MD.

Sandborg, M., Alm Carlsson, G., 1992. Influence of X-ray energy spectrum, contrasting detail and detector on the signal-to-noise ratio (SNR) and detective quantum efficiency (DQE) in projection radiography. Phys. Med. Biol. 37, 1245–1263.

Sandborg, M., 1993a. Effective use of X-rays in diagnostic radiology: guidance for the optimisation of image quality and absorbed dose in the patient by use of a Monte Carlo computational model of the imaging system. Thesis No. 389, Linköping University, Linköping, Sweden.

Sandborg, M., Dance, D. R., Alm Carlsson, G., Persliden, J., 1993b. Monte Carlo study of grid performance in diagnostic radiology: factors which affect the selection of tube potential and grid ratio. Br. J. Radiol. 66, 1164–1176.

Sandborg, M., Dance, D. R., Persliden, J., Alm Carlsson, G., 1994a. A Monte Carlo program for the calculation of contrast, noise and absorbed dose in diagnostic radiology. Comput. Methods Programs Biomed. 42, 167–180.

Sandborg, M., Dance, D. R., Alm Carlsson, G., Persliden, J., 1994b. Monte Carlo study of grid performance in diagnostic radiology: task dependent optimisation for screen film imaging. Br. J. Radiol. 67, 76–85.

Sandborg, M., Christoffersson, J. O., Alm Carlsson, G., Almén, T., Dance, D. R., 1995. The physical performance of different X-ray contrast agents: Calculations using a Monte Carlo model of the imaging chain. Phys. Med. Biol. 40, 1209–1224.

Shrimpton, P. C., Jones, D. G. and Wall, B. F., 1981. A re-evaluation of the relationship between exposure-area product ($R\,cm^2$) and the energy imparted to the patient during diagnostic radiological examinations. *CEC (Commission of the European Communities) Radiation Protection: Patient Exposure to Radiation in Medical X-ray Diagnosis: Possibilities for Dose Reduction*. Report EUR7438. CEC, Luxembourg.

Shrimpton, P. C., Wall, B. F., 1982. An evaluation of the Diamentor transmission ionisation chamber in indicating exposure-area product ($R\,cm^2$) during diagnostic radiological examinations. Phys. Med. Biol. 27, 871–878.

Shrimpton, P. C., Wall, B. F., 1983. Comparison of methods for estimating the energy imparted to patients during diagnostic radiological examinations. Phys. Med. Biol. 28, 1160–1162.

Shrimpton, P. C., Wall, B. F., Jones, D. G., Fisher, E. S., 1984. The measurement of energy imparted to patients during diagnostic X-ray examinations using the Diamentor exposure-area product meter. Phys. Med. Biol. 29, 1199–1208.

Shuping, R. E., Judy, P. F., 1977. Energy absorbed in calcium tungstate X-ray screens. Med. Phys. 4, 239–243.

Stargardt, A., Angerstein, W., 1975. Über die Streustrahlenverminderung bei der Röntgenvergrösserungstechnik. Fortschr. Röntgenstr. 123, 364–369.

Stenström, B., Henriksson, C. O., Karlsson, L., Sarby, B., 1986. Energy imparted from intraoral radiography. Swed. Dent. J. 10, 125–136.

Stenström, B., Henriksson, C. O., Karlsson, L., Sarby, B., 1987. Effective dose equivalent from intraoral radiography. Swed. Dent. J. 11, 71–77.

Stenström, B., Karlsson, L., 1988. Collective doses to the Swedish population from panoramic radiography and lateral cephalography. Swed. Dent. J. 12, 161–170.

Svahn, G., 1977. Diagnostic X-ray spectra: A study of the effects of high tension ripple, large X-ray tube currents, extrafocal radiation and anode angulation with Ge(Li) spectroscopy. Thesis, Lund University, Lund, Sweden.

Swank, R. K., 1973. Absorption and noise in X-ray phosphors. J. Appl. Phys. 44, 4199–4203.

Tapiovaara, M. J., Sandborg, M., 1995. Evaluation of image quality in fluoroscopy by measurements and Monte Carlo calculations. Phys. Med. Biol. 40, 589–607.

Tapiovaara, M. J., Wagner, R. F., 1985. SNR and DQE analysis of broad spectrum X-ray imaging. Phys. Med. Biol. 30, 519–529.

Tapiovaara, M., Lakkisto, M. and Servomaa, A., 1997. PCXMC: A PC-based Monte Carlo program for calculating patient doses in medical X-ray examinations. STUK-A139. Finnish Centre for Radiation and Nuclear Safety, Helsinki.

Wall, B. F., Harrison, R. M. and Spiers, F. W., 1988. Patient Dosimetry Techniques in Diagnostic Radiology. IPSM Report 53. The Institute of Physical Sciences in Medicine, York.

Vyborny, C. J., 1976. The speed of radiographic screen film systems as a function of X-ray energy and its effects on radiographic contrast. Thesis, University of Chicago.

Wagner, R. F., 1977. Noise equivalent parameters in general medical radiography: The present picture and future pictures. Photogr. Sci. Eng. 21, 252–262.

Wu, X., Barnes, G. T., Tucker, D. M., 1991. Spectral dependence of glandular tissue dose in screen-film mammography. Radiology 179, 143–148.

Zoetelief, J., Jansen, J. T. M., 1995. Calculation of air kerma to average glandular tissue dose conversion factors for mammography. Radiat. Prot. Dosim. 57, 397–400.